DTIC FILE COPY

(2)

SECURITY CLASSIFICATION OF THIS PAGE

PAGE

1a. REPORT SECURITY CLASSIFI | TIVE MARKINGS

2a. SECURITY CLASSIFICATION. | AD-A226 548 | TION/AVAILABILITY OF REPORT

2b. DECLASSIFICATION/DOWNGI | Unlimited

4. PERFORMING ORGANIZATION REPORT NUMBER(S) | 5. MONITORING ORGANIZATION REPORT NUMBER(S)

6a. NAME OF PERFORMING ORGANIZATION: State University of New York at Stony Brook | 6b. OFFICE SYMBOL (If applicable) | 7a. NAME OF MONITORING ORGANIZATION: Same as 8A

6c. ADDRESS (City, State and ZIP Code): Department of Physics, SUNY, Stony Brook, N. Y. 11794 | 7b. ADDRESS (City, State and ZIP Code): Same as 8B

8a. NAME OF FUNDING/SPONSORING ORGANIZATION: ONR | 8b. OFFICE SYMBOL (If applicable) | 9. PROCUREMENT INSTRUMENT IDENTIFICATION NUMBER: N00014-84-C-0261

8c. ADDRESS (City, State and ZIP Code): 800 N. Quincy Street, Arlington, Virginia 22217 | 10. SOURCE OF FUNDING NOS.

PROGRAM ELEMENT NO.	PROJECT NO.	TASK NO.	WORK UNIT NO.

11. TITLE (Include Security Classification): Experimental Studies of Josephson Effect

12. PERSONAL AUTHOR(S): James Lukens

13a. TYPE OF REPORT	13b. TIME COVERED	14. DATE OF REPORT (Yr., Mo., Day)	15. PAGE COUNT
Final	FROM 840315 TO 890930	900906	21 pages

16. SUPPLEMENTARY NOTATION: reprints enclosed

17. COSATI CODES			18. SUBJECT TERMS (Continue on reverse if necessary and identify by block number)
FIELD	GROUP	SUB. GR.	Josephson Devices, SQUID

19. ABSTRACT (Continue on reverse if necessary and identify by block number)

See attached summary

DTIC ELECTE SEP 12 1990 S E D

20. DISTRIBUTION/AVAILABILITY OF ABSTRACT

UNCLASSIFIED/UNLIMITED ☒ SAME AS RPT. ☐ DTIC USERS ☐

21. ABSTRACT SECURITY CLASSIFICATION: Unclassified

22a. NAME OF RESPONSIBLE INDIVIDUAL	22b. TELEPHONE NUMBER (Include Area Code)	22c. OFFICE SYMBOL
James Lukens, Project Director	(516)632-8081	

DD FORM 1473, 83 APR EDITION OF 1 JAN 73 IS OBSOLETE.

SECURITY CLASSIFICATION OF THIS PAGE

90 09 12 07

OFFICE OF NAVAL RESEARCH

FINAL TECHNICAL REPORT

for

15 March 1984 through 30 September 1989

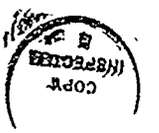

for

Contract N00014-84-C-0261

Task No. NR 604-004

Josephson Devices

James Lukens

The Research Foundation of
State University of New York
P.O. Box 9
Albany, New York 12201

Accession For	
NTIS GRA&I	X
DTIC TAB	☐
Unannounced	☐
Justification	
By	
Distribution/	
Availability Codes	
Dist	Avail and/or Special
A-1	

Reproduction in whole, or in part, is permitted for any purpose of the United States Government.

* This document has been approved for public release and sale; its distribution is unlimited.

Final report on ONR contract #N00014-84-C-0261

Summary of work completed under the contract

During the course of this contract, research has been conducted in three distinct areas, all involving the Josephson effect:

A. Development of Josephson junction arrays as tunable sources of microwave through submillimeter radiation,

B. Conformation of general relativistic effects, equivalent to the red shift, for charged particles, and

C. Studies of the quantum mechanics of macroscopic variables, in particular of the flux linking a SQUID.

The fundamental studies of Josephson oscillators A.), which had been supported under previous ONR contracts, were concluded during the first part of the contract. The present status of this work is discussed in detail in the reprint attached as reference A. The success of this work has lead to very active ongoing research programs in my laboratory, supported by several sources to develop technical applications of these oscillators. In particular, techniques for coupling junctions distributed over many wavelengths were developed and applied to the design of a broadly tunable submillimeter source generating 7μW of power at 400GHz. In addition, recent results on frequency agile microwave sources demonstrate modulation of a 16GHz carrier over 3GHz at modulation frequencies in excess of 500MHz.

Our focus during the middle years of the contract was on B.), the study of effects predicted by general relativity on charged particles moving through a gravitational field. These experiments, which are described in the reprint in appendix B, produced the first demonstration that the electrochemical potential difference between two superconducting wires varies with gravitational potential (by about 1 part in 10^{16} per meter in the earth's field). This effect is essentially the equivalent for charged particles of the well known gravitational red shift for photons. Use was made of essentially ideal Josephson effect "batteries" phase-locked to a microwave source to establish precisely related *EMF*s at different heights. As part of this work techniques were developed to measure potential differences of 10^{-22}V.

During the final phase of the contract, we began work to test predictions that macroscopic variables, such as the flux through a SQUID loop, display quantum

mechanical properties such as tunneling and coherent superposition of the flux wave functions belonging to different states. This work has been continued under a subsequent ONR grant and has produced the first evidence that quantum theory for transitions between the fluxoid states in a degenerate two level SQUID is correct. The results under this contract are presented in the reprint in appendix C. Here a novel technique is demonstrated for using a two junction composite SQUID to make what is essentially a "man made atom" with energy levels and lifetime which can be controlled *in situ* by the experimenter.

APPENDIX A

CHAPTER 4

Josephson Arrays as High Frequency Sources

JAMES LUKENS

Department of Physics
State University of New York
Stony Brook, New York

1. Introduction 135
2. Single-Junction Sources 137
2.1. Small Junctions 137
2.2. Fluxon Oscillators (Wide Junctions). 140
2.3. Radiation Linewidth 141
3. Arrays 142
4. Phase-Locking 146
5. Phase-Locking in Arrays. 149
5.1. Locking Strength within the RSJ Model 149
5.2. Radiation Linewidth of Arrays. 153
5.3. Effects of Capacitance on Phase-Locking in Arrays 156
6. Distributed Arrays 159
7. Prospects for the Future 163
Acknowledgments. 165
References 165

1. Introduction

There is a rapidly developing need for compact submillimeter sources for use in such applications as satellite communications and receivers for astronomical observation. Fundamental solid-state oscillators such as Gunn or IMPATT diodes are presently limited to the millimeter wave range, leaving such bulky and power hungry sources as carcinotrons and CO_2 lasers, which operate in some parts of the submillimeter range.

Josephson junctions are natural voltage-controlled oscillators, and it has been recognized since the discovery of the Josephson effect that these junctions have the potential for filling this source gap at least up to frequencies of several terahertz. As the Josephson equations imply, the average frequency of supercurrent oscillation ν_0, which we call the Josephson frequency, in a

junction is related to the dc component $\bar{V}$ of the voltage across the junction only through fundamental constants,

$$\bar{V} = \frac{h}{2e}\nu_0, \tag{1.1}$$

where e is the charge on the electron and h is Planck's constant, so $2e/h = 483$ GHz/mV. Indeed this remarkable result has been shown [1.2] to be independent of the materials or structure of the junction to better than 1 part in 10^{16}. One would thus hope that Josephson junctions would be useful tunable sources operating up to the superconducting gap frequency—a few THz for conventional superconductors and perhaps tens of THz for the new high-T_c materials.

Unless the junction voltage is constant in time, i.e., $V(t) = \bar{V}$, Eq. (1.1) does not necessarily imply a pure sinusoidal oscillation with frequency proportional to the dc voltage. In practice, at high frequencies, it is usually easier to control the junction's bias current than its voltage. Indeed, there are many examples in the literature, such as chaotic behavior or periodic mode-locking to resonant structures, where, even though Eq. (1.1) is satisfied, almost none of the power generated by the junction is at the frequency ν_0. Although a great deal of work in many laboratories has gone into the development of practical sources based on the Josephson effect, the serious problems related to the very low power and source impedance of individual junctions in addition to that of obtaining spectrally pure oscillation at the Josephson frequency have been difficult to surmount. One technique for overcoming these problems, which will be the focus of this chapter, is to use arrays of junctions in place of single junction sources. The discussion presented here has evolved from a lecture at the Nato Advanced Study Institute on Superconducting Electronics [3].

First, the properties of single junction sources will be reviewed in order to get a perspective on the problems to be solved. After a brief look at the performance expected from idealized arrays, perturbative techniques for analyzing arrays will be developed based on the resistively shunted junction (RSJ) model. While this model is clearly only approximately correct for real tunnel junctions, it can produce analytic results useful for achieving an insight into the design of coherent arrays. These results have proven to provide a very good description of many of the experiments to date. The final parts of this chapter will present a number of recent results for practical array sources where the junctions are distributed over many wavelengths as well as speculations on future directions for research.

2. Single-Junction Sources

2.1. *Small Junctions*

The properties of single-junction sources will be described first in order to see where arrays may be useful. The RSJ model (Fig. 1a) with $C = 0$ will be used to describe the junction's behavior since, for this case, analytic solutions exist which provide a useful insight. See, for example, [4], Chapter 4. When the bias current I_b is increased above I_c, the junction's phase ϕ begins to increase with time, producing an oscillating supercurrent (since $I_s = I_c \sin\phi$) and consequently an oscillating voltage. For I_b near I_c, the voltage waveform is nearly a spike, having a large harmonic content. As I_c is increased the higher harmonic content of the waveform decreases, giving a nearly sinusoidal wave for $\bar{V} \geq V_c \equiv I_c R_J$. The amplitudes of the harmonics are given by

$$\tilde{V}_n \equiv V_c \tilde{v}_n = V_c \frac{2\bar{v}}{[(1 + \bar{v}^2)^{1/2} + \bar{v}]^n}, \tag{2.1}$$

where $\bar{v} \equiv \bar{V}/V_c$ and $i \equiv I_b/I_c$ and for the RSJ model $\bar{V} = (i^2 - 1)^{1/2}$. Also, $\omega_c \equiv 2\pi V_c/\Phi_0$. This waveform approaches a nearly pure sinusoid for $\bar{v} > 1$. Since for most applications one would like a reasonably sinusoidal source, we will impose the constraint that $\bar{v} \geq 1$ at the desired operating frequency.

Since the junction impedance at the Josephson frequency is $Z \approx R_J$ for $\bar{v} \geq 1$, at high frequencies the junction can be viewed as an oscillator of

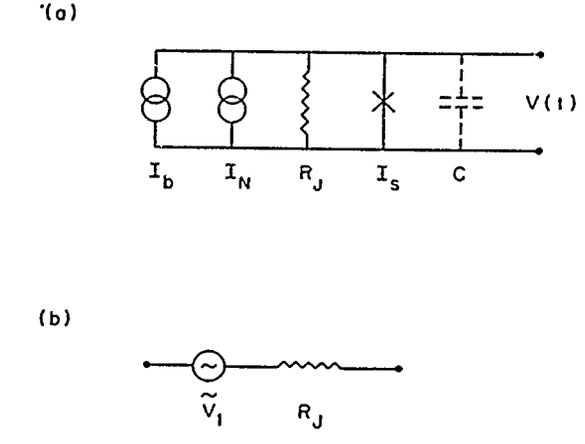

Fig. 1. (a) Equivalent circuit model for resistively shunted junctions (RSJ) with bias current I_b, noise current I_N, shunt resistance R_J, capacitance C, and supercurrent $I_s = I_c \sin\phi$. (b) Equivalent circuit for frequencies near ν_0.

amplitude $\tilde{V}_1$ at the Josephson frequency in series with R_J as shown in Fig. 1b. The power available to a matched load from a single junction is then

$$P_1(v) = \frac{1}{8}\frac{\tilde{V}_1^2}{R_J} \to \frac{1}{8} I_c^2 R_J, \qquad \bar{v} \geq 1. \tag{2.2}$$

There are limits on both I_c and R_J that limit the maximum power obtainable at a given frequency. The discussion so far has assumed that the junction is one dimensional; that is, the phase difference between the electrodes is independent of the position on the electrode transverse to the direction of tunneling current flow. This, in general, means that the dimensions of the junction must be limited to assure a constant current density. Since the natural scale over which current density varies in the junction is the Josephson penetration depth $\lambda_J^2 = h/(2e\mu_0 d J_c)$ (where d is the magnetic thickness of the barrier), keeping the junction's dimensions of order λ_J will assure the required uniformity. For an in-line junction with critical current density J_c (shown in Fig. 2) over a ground plane, the current is confined (on the x-axis) within about $2\lambda_J$ of the end of the junction giving a maximum effective critical current in zero field of $I_c \approx 2\lambda_J w J_c$, where w is the width of the junction [5]. As long as the current feeding the junction is uniform across the width of the junction (y-axis), a solution exists in which the current density within the junction is also constant across its width for arbitrarily wide junctions.

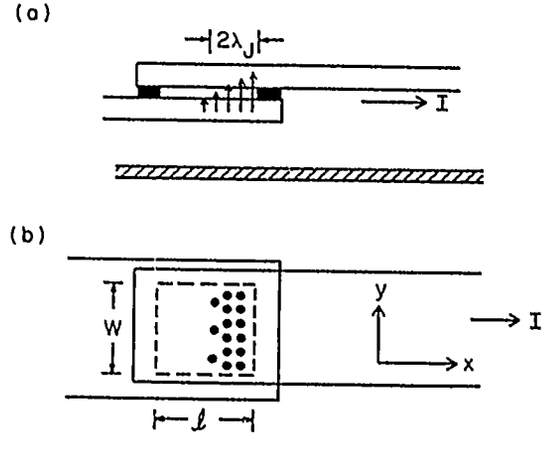

Fig. 2. Diagram of an in-line junction. (a) Edge view showing $J_c(x)$ concentrated within $2\lambda_J$ of the end of the junction. (b) Top view. Tunnel barrier is enclosed by dashed lines. Regions of non-zero tunneling current are shown by ●.

At some point instabilities will develop in this uniform solution and limit the junction's width in practice. A very conservative estimate for this maximum stable width would be $2\lambda_J$. Then, since $\lambda_J^2 \propto 1/J_c$, the maximum critical current for a given material would be independent of J_c and equal to about 4 mA for niobium. At the other extreme, very wide in-line junctions are known to have flux flow across the junction. One might expect this sort of instability to develop when the electromagnetic wavelength λ_{em} in the junction was equal to twice the junction width, that is, at the first zero field step, since for this condition there will be where strong coupling between the Josephson and fluxon oscillations. Indeed, it has been observed [6] that the phase-locking of junctions in voltage standard arrays to external radiation decreases abruptly for wider junctions. If the first instability is the first zero field step, then the maximum junction width will be given by

$$w_{cm} = \frac{1}{2\nu(\mu_0 d C_s)^{1/2}}, \tag{2.3}$$

where C_s is the specific capacitance. This width is independent of J_c but varies inversely with frequency. Thus, the maximum critical current for this condition would depend on the critical current density but would decrease with frequency. For example. a niobium junction with a critical current density of 10^5 A/cm^2 would have a maximum stable critical current of $I_c \approx$ 7.6 mA/ν [THz].

Having fixed I_c, R_J should be adjusted using a shunt resistor depending on the desired operating frequency and limited, of course, by the material-dependent intrinsic I_cR_J product of the junction. The condition $\bar{v} \geq 1$ for a sinusoidal waveform limits the maximum resistance for a given I_c and frequency ν. On the other hand, if R_J is reduced below the value for which $\bar{v} = 1$, Eq. (2.2) indicates that the power will decrease. Thus, one should select the shunt resistance such that $R_J \approx \nu\Phi_0/I_c$ giving

$$P_1(\nu) \approx \frac{1}{8}\nu\Phi_0 I_c. \tag{2.4}$$

Figure 3 illustrates the source resistance, critical current, and available power as a function of frequency for single-junction sources subject to the width constraints discussed above. For junctions with $w = 2\lambda_J$, one sees that the maximum single junction power is proportional to frequency with

$$P_1(\nu) \approx 1(\nu\ [\text{THz}])\ \mu\text{W} \tag{2.5}$$

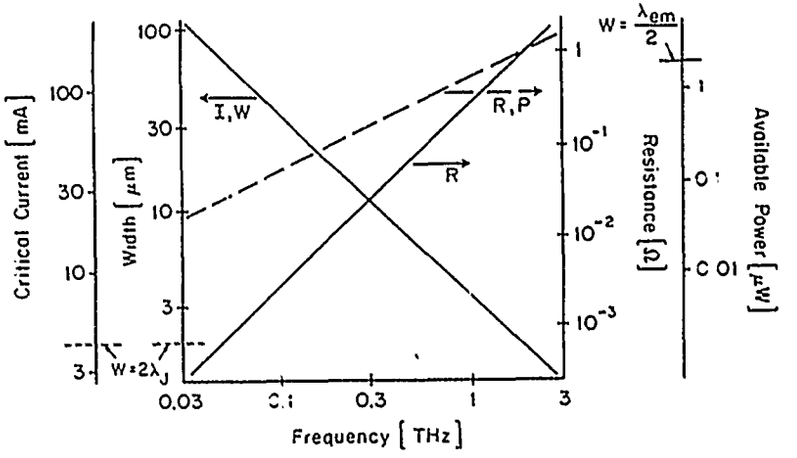

Fig. 3. Properties of single-junction sources designed for maximum available power at a given frequency subject to the width constraints $w = 2\lambda_J$ (··· narrow) and $w = 0.5\ \lambda_{em}$ (— wide); for both cases, $J_c = 10^3$ A/cm^2 and length is $2\lambda_J = 2$ μm. For narrow junctions, the frequency-independent values of I_c and w are indicated on the axes (···). The available power of the wide junction is also frequency independent as shown on the power axis.

Thus, for example, one might expect a maximum power of about 1 μW at 1 THz. While this is sufficient for some applications, it is about the limit with proportionately less power available at lower frequencies. Also the source impedance for this 1 μW source would be less than an ohm. This would require a substantial transformer ratio for typical loads and could be a problem if wide tuning were desired. Junctions with $w = \lambda_{em}/2$ have the potential for delivering above a microwatt at lower frequencies but at the expense of even lower source impedances.

2.2. *Fluxon Oscillators (Wide Junctions)*

There are several groups that have reported significant power levels at frequencies up to several hundred gigahertz from fluxon propagation in very wide junctions. While the focus of this chapter will be on series arrays of junctions small enough to have a spacially uniform current density, we will briefly review these results for fluxon oscillators for the perspective that they provide on the possible advantages and disadvantages of this type of source.

Significant power has been observed from two different types of fluxon oscillators. The first, which uses unidirectional flow, has been studied mainly in Japan [7,8]. In this type of oscillator, a magnetic field is applied in the plane

of the junction, along the x-axis (Fig. 2) to form flux vortices or fluxons in the junction. The bias current then forces the vortices to flow across the junction (along the y-axis) along the transmission line formed by the base and counter electrodes. If the bias current is increased until the vortices are moving near the speed of light in the junction, voltage and thus the frequency become insensitive to small changes in the bias, i.e., the junction has very low differential resistance. The frequency can be tuned over a wide range by varying the vortex density in the junction by changing the applied field. It is estimated [8] that of the order of a microwatt of power should be available from such oscillators at frequencies ranging from about 100 GHz to 1 THz, and powers of this magnitude coupled to an SIS detector at the end of the junction transmission line have been reported up to 400 GHz. A problem associated with this type of oscillator is that the characteristic impedance, which is that of the transmission line formed by the junction, is in general quite low. Transformers have been developed [7] to couple power more efficiently to higher impedance loads and have succeeded in coupling about 0.1 μW to a 1 Ω load at 200 GHz. The penalty for using these resonant transformers, however, is that the tuning range is severely restricted.

The second type of fluxon oscillator, which has been studied primarily by groups in Europe, has a similar geometry but uses a high Q resonant junction. These resonant fluxon oscillators are operated on their zero field steps, the operating frequency being determined by the dimensions of the junction rather than an applied field. Two groups have recently reported detecting power levels of the order of 0.1 μW from such junctions. One group [9] reported radiation at 75 GHz using on-chip detection with small junctions. The oscillator junctions had a transmission line impedance of 1 Ω and an estimated available power of about 0.1 μW. Simulations show a steplike structure in junction's phase vs. time indicating a large harmonic content to the radiation as one might expect from the picture of fluxons shuttling back and forth in the junction. A second group [10,11] reported radiation near 10 GHz from an array of resonant fluxon oscillators in which a significant degree of phase-locking among the junctions was observed. In this case, the radiation was coupled to a detector outside of the cryostat. Power levels of over 0.1 μW in a 50 Ω load were reported. In smaller arrays, where more complete locking could be achieved, linewidths of several kilohertz were observed.

2.3. *Radiation Linewidth*

A final consideration related to single junction sources is their linewidth. The linewidth of the Josephson radiation is determined by frequency modulation

due to low frequency voltage noise across the junction [12] with frequencies up to about the linewidth $\Delta\nu$ being important. In terms of the current noise in the junction,

$$\Delta\nu = \frac{1}{2}\left(\frac{2\pi}{\Phi_0}\right)^2 S_I(0) R_d^2. \tag{2.6}$$

Here $S_I(0)$ is the low frequency current spectral density, and R_d is the differential resistance at the operating voltage. If $S_I(0)$ is just the Johnson noise current of the junction resistance R_J and $R_d \approx R_J$, then $\Delta\nu \approx 160$ MHz per ohm of junction resistance at 4 K. This is only a rough guide, since $S_I(0)$ will in general be increased due to such things as $1/f$ noise prevalent in high J_c junctions, as well as to down-converted quantum noise from near the Josephson frequency. On the positive side, since only low frequency noise is important in determining $\Delta\nu$, one can in principle make the linewidth arbitrarily small by shunting the junction at low frequencies without reducing its high frequency impedance. This technique has been successfully used [13], although it can have drawbacks such as the introduction of instabilities or chaotic behavior.

Another technique for linewidth reduction is to reduce the differential resistance of the junction at the operating point through coupling to a resonant structure. An example of this is the fluxon oscillations in resonant wide junctions discussed above. These junctions can have very low differential resistance when biased on their zero field steps. The situation with unidirectional flux-flow is more complex. While the differential resistance is also small at the operating point, the junctions are tunable by varying the flux, so the linewidth will to some extent be affected by fluctuations of the flux linking the junctions, perhaps more than by spacially uniform fluctuations in the bias current.

One can summarize the properties of single junction sources by saying that, in general, such sources have either too little power, too low an impedance, too broad a linewidth, or all of the above, although the power and impedance begin to become useful for some applications as terahertz frequencies are approached. Next we will take a brief, rather elementary look at small junction arrays to see to what extent the replacement of single junctions by arrays of junctions might solve these problems.

3. Arrays

Interest in Josephson arrays was sparked in the late 1960s by experiments of Clark [14] and a paper by Tilley [15] who predicted superradiance in such arrays, much as in a collection of atoms in a cavity. One signature of this

superradiance was a prediction that the output power would scale as the square of the number of junctions. This led to a hope—rather naive in retrospect—that significant power levels could be obtained from Josephson junctions simply by connecting a large number of junctions together without worrying in detail about just how they were coupled. The initial experiments were done by Clark [14,16] on two-dimensional arrays of superconducting balls. which were Josephson-coupled through their oxide coating as shown in Fig. 4b. Indeed, evidence of interactions among the junctions was seen; however, experiments of this type have never produced significant levels of power. As will be seen later, when the details of how junctions phase-lock is discussed, for arrays of this type power is mostly dissipated in the array itself. The development of Josephson-effect arrays, involving hundreds of workers, has been covered in detail in two review papers by Jain *et al.* [17] and Lindelof and Hansen [18] and more recently in a book by Likharev [4]. Readers are referred to these sources for a comprehensive review.

In more recent work, including successful attempts to obtain increased power from arrays of junctions, the junctions are simply treated as classical oscillators, i.e., the junction's current and phase are taken to be classical variables as in the discussion of single-junction sources above. This is the approach taken throughout this chapter. It is worth emphasizing the distinction between the present work based on the classical picture and the initial discussion of Josephson arrays in terms of superradiance, since much confusion has been caused over the years by not fully appreciating this distinction. This confusion has been compounded by the fact that there have been observations of the power from arrays increasing as N^2, as predicted for superradiance. As far as we know, all these observations can be explained in terms of purely classical circuit analysis, as will be seen, for example, below.

Probably the simplest example of the advantages to be gained from arrays of junctions can be seen by considering the one-dimensional array shown in Fig. 4a. Here a number of junctions are connected, e.g., by a transmission line, in series with each other and with the load R_L to be driven, so that the rf current generated by a junction flows through all of the other junctions and the load. Representing each junction by its high frequency equivalent circuit (Fig. 1b), which to first order is not affected by the rf current, one sees that the array impedance can be matched to the load by taking the number of junctions to be $N = R_L/R_J$, thus solving the low impedance problem of single junction sources. For now, it is simply assumed that all of the junctions will oscillate at the same frequency and in-phase. The discussion of the conditions needed for such phase-locking will occupy much of the remaining sections of this chapter. It will also be assumed for now that the circuit dimensions are

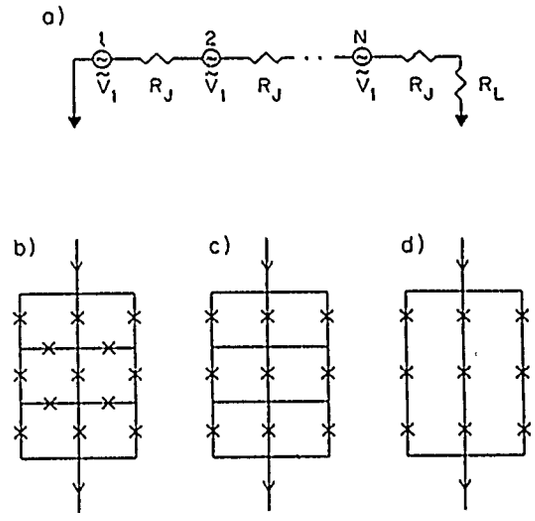

Fig. 4. (a) High frequency equivalent circuit for a one-dimensional array. (b)–(d) Possible junction connections for two-dimensional arrays.

small compared to the wavelength in the transmission line at the frequency of operation so that the lumped circuit approximation can be used. The constraints on I_c and R_J discussed in Section 2 can then be used to estimate the number of junctions needed to match a 50 Ω load to an array designed to operate near a frequency ν, giving

$$N = \frac{R_L}{R_J} \approx \begin{cases} \dfrac{100}{\nu\,[\mathrm{THz}]}, & w = 2\lambda_J, \\ \dfrac{200}{\nu\,[\mathrm{THz}]^2}, & w = \dfrac{\lambda_{em}}{2}. \end{cases} \tag{3.1}$$

Here the two estimates for N correspond to the limits on the width of the small junctions as discussed in Section 2, taking $J_c = 10^5$ A/cm^2.

The available power from this one-dimensional array is just N times that available from a single junction in the array. Which for the 50 Ω load is

$$P_N = NP_1 \approx \frac{1}{8} I_c^2 R_L \approx \begin{cases} 0.1\ \mathrm{mW}, & w = 2\lambda_J, \\ \dfrac{0.4\ \mathrm{mW}}{\nu\,[\mathrm{THz}]^2}, & w = \dfrac{\lambda_{em}}{2}. \end{cases} \tag{3.2}$$

If it is possible to match an array of any size to a load using a transformer, then the dependence of power on array size is linear in the number of junctions. The

enormous impedance mismatch between a single junction and a typical load makes the use of transformers problematical, especially if much tuning range is to be preserved. Without transformers, situations occur where, when the number of junctions is varied, the load power varies as N^2. For example, this happens when the number of junctions is increased but the total array impedance is small compared to that of the load. An N^2 dependence also occurs if an array of junctions with $I_c < I_{cmax}$ is matched to the load by reducing R_j as N increases such that NR_j and I_cR_j remain constant. Thus, for many practical situations, the power from arrays is expected to increase as N^2. These situations are clearly purely classical in nature but are sometimes confused with superradiance.

Next, one could ask whether anything is gained by replacing the one-dimensional array by a two-dimensional array, as in Figs. 4b–d. We imagine making such an array by replacing each junction in Fig. 4a by a parallel (transverse to the rf current) string of junctions, M junctions wide as in Fig. 4c. If all of these junctions were identical and all oscillated in phase, this would be equivalent to replacing each junction in Fig. 4a with a junction having $I_c' = MI_c$ and $R_j' = R_j/M$. One would then need M times as many of these series junctions to match the load; thus, the power delivered to the load would be increased by a factor M^2.

As an example, at 1 THz approximately 100 junctions with $w = 2\lambda_j$ would be required in a one-dimensional array to match a 50 Ω load, producing a power of 0.1 mW. If a two-dimensional array were used with a width $M = 100$, then the matched array would have 10^6 junctions and deliver 1 W of power. It is not difficult to fabricate a million-junction array with modern lithographic techniques. The real question is whether all of the junctions could be made to oscillate in phase as assumed above, particularly since the motivation for thinking about a two-dimensional array is that the useful critical current of a single junction is limited due to phase instabilities that arise at larger values of I_c. Similar power estimates are obtained for the configuration shown in Fig. 4d.

The arrays discussed above (Figs. 4a, c, d) could all be called linear arrays since for proper operation the phase should vary only in one direction, even in the two-dimensional arrays. It is important to distinguish this situation from truly two-dimensional arrays (Fig. 4b) where the phase varies in both dimensions. There has been a great deal of very interesting work, primarily to study phase transitions, in these latter arrays. This work will be completely ignored here since it really does not address the problems related to using Josephson arrays as radiation sources.

4. Phase-Locking

It should be clear from the brief discussion above that the real key to the usefulness of arrays is how, or if, the junctions phase-lock. Even if all of the junctions are identical, one must still ask if the "uniform phase" condition (in which all junctions have the same phase relative to the locking current) is a solution, and if so, is it a stable solution. If there is such a stable solution, the next problem is to find out what happens if all of the junctions are not identical. In real arrays, there is always some degree of scatter in the junction parameters, e.g., the critical current, as well as random noise, which tend to make the junctions of the array oscillate at different frequencies.

It is possible to get much insight into both the stability and strength of phase-locking in arrays by considering the well-known phenomenon of a single-junction phase-locking to external radiation. We still start by using perturbation theory to study the effects of external radiation on an RSJ for which analytic solutions are available. Later, the effects of junction's capacitance in the low $\beta_c(\beta_c \equiv \omega_c R_j C \leq 1)$ limit will be included. The perturbation techniques used are standard and have been applied to Josephson junctions by several authors [19,20]. Here the key ideas of the theory will be reviewed briefly and then applied to the phase-locking problem. To begin, a quantity related to the junction phase ϕ, called the "linearized phase", is defined by

$$\Theta = \hat{\omega}t, \tag{4.1}$$

where $\hat{\omega}$ is the junction's frequency averaged over a time long compared to a period of a Josephson oscillation, yet short enough to respond to the low frequency noise and modulation. The $\hat{}$ symbol is used in general to indicate averaging over the time scale which is long compared to $1/\omega$. The success of the perturbation theory depends on the wide separation of the Josephson frequency from the low frequency currents that are important in fixing the linewidth and oscillation frequency.

The essential results of the perturbation theory are shown schematically in Fig. 5 where the junction is represented by an equivalent circuit with two parts, one for the high frequency (HF) (near ω) behavior, and the second modeling the low frequency (LF) response. The high frequency circuit consists of the Josephson oscillator (with amplitude $\tilde{V}_1$ given by Eq. (2.1) and frequency ω) and the source impedance R_j. This HF section is coupled to the LF section through ω, which is determined by the LF voltage through the Josephson equation (1.1).

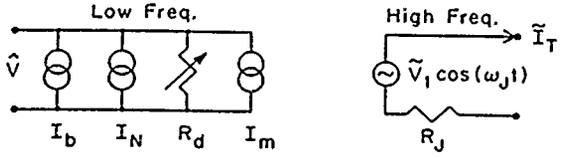

Fig. 5. Equivalent circuit for the RSJ model from perturbation theory. Low frequency (LF) section models response for $\omega \ll \omega_J$ ($\omega_J = 2\pi\hat{V}/\Phi_0$) and is coupled to the high frequency (HF) section by the mixing current I_m—see text. The HF section contains the Josephson oscillator $\tilde{V}_1 \cos \omega_J t$ and source impedance R_J. The perturbation consists of an rf current $\tilde{I}_T$ with $\omega \sim \omega_J$ flowing through the HF terminals.

The perturbations that we wish to consider are caused by an rf current $\tilde{I}_T$ with a frequency near ω flowing through the HF terminals. This in turn affects the LF voltage (and thus ω) through the presence of a "mixing current",

$$I_m = \alpha\overbrace{(2\tilde{I}_T \cos \Theta)}, \tag{4.2}$$

in parallel with the bias and noise currents on the LF side. Here α is the conversion coefficient, which is given in the RSJ model as

$$\alpha = \frac{1}{2(1 + \bar{v}^2)^{1/2}}. \tag{4.3}$$

The cause of this perturbation might, for example, be either an external rf current source or a load placed across the HF terminals, or both. So

$$\hat{\omega} = \hat{\omega}_u(\hat{I} + I_m), \tag{4.4}$$

where the subscript u refers to the value of the variable ω in the absence of the HF perturbation. In other words, in the presence of a HF perturbation, the junction will oscillate at the same frequency as an unperturbed junction biased with a current equal to the sum of the bias and mixing currents in the perturbed junction.

In order to apply this technique to understand the phase-locking of a junction to external radiation, we take the perturbing rf current to be that due to an external current source with amplitude I_e and frequency ω_e near ω, so

$$\tilde{I}_T = I_e \cos \omega_e t. \tag{4.5}$$

This gives a mixing current

$$I_m = \alpha I_e \cos \delta\Theta, \tag{4.6}$$

where $\delta\Theta \equiv \Theta - \omega_e t$.

Equation (4.4) is actually a differential equation for Θ which can be rewritten by expanding ω (I) about I_b using the differential resistance of the unperturbed junction and remembering (Eq. (4.1)) that $\dot{\Theta} = \hat{\omega}$. Thus,

$$\frac{\Phi_0}{2\pi R_d}\dot{\Theta} - \alpha I_e \cos \delta\Theta = \frac{\Phi_0}{2\pi R_d}\omega_u(\hat{I}). \tag{4.7}$$

If a new variable, $\theta \equiv \Theta - \omega_e t - \pi/2$ is defined, then (4.7) becomes

$$\frac{\Phi_0}{2\pi R_d}\dot{\theta} + I_L \sin \theta = \delta I, \tag{4.8}$$

where

$$I_L = \alpha I_e \tag{4.9}$$

and

$$\delta I = I_b - I_{be}. \tag{4.10}$$

That is, δI is the difference between the actual bias current and the bias current I_{be} that would make the unperturbed junction oscillate at frequency ω_e. This equation is just the familiar equation for the phase of a RSJ with critical current I_L, resistance R_d, and bias current δI; hence, the solutions are well known.

The main result that we need is the locking strength, that is, the range of bias current over which $\dot{\theta} = 0$. Equation (4.8) clearly has a constant θ solution for $-I_L \le \delta I \le I_L$, with $0 \le \Theta - \omega_e t \le \pi$. Thus, as seen in Fig. 6a, $\bar{V}$ remains constant over a range of bias currents $2I_L$ about the bias current I_{be} for which

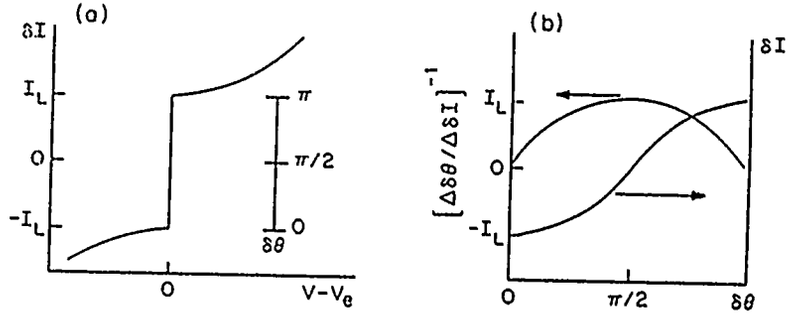

Fig. 6. (a) Junction I–V curve in neighborhood of a radiation-induced step. (b) Phase-locking stability along step, $[\partial(\delta\Theta)/\partial(\delta I)]^{-1}$. Note greatest stability is for $\delta\Theta = \pi/2$. The region $0 > \delta\Theta > -\pi$ is unstable.

the unperturbed junction would have frequency ω_c. Note that this locking strength could also be expressed in terms of the variation in I_c (since I_{bc} is a function of I_c), which is possible at fixed bias without losing phase-lock. This latter view is more relevant for arrays in which we may wish to bias a string of junctions with a common current and ask how large a scatter (e.g., in I_c) can be tolerated. In this sense, a junction is most strongly locked when biased in the center of the current step where the difference between the phase of the junction's oscillation and that of the external radiation is $\pi/2$, i.e., $\delta\Theta = \pi/2$. For this bias, the greatest deviation of I_c is possible in an arbitrary direction. The condition that the phase shift be $\pi/2$ for strongest locking has important implications for the design of arrays, as we shall see below. Another measure of locking strength is the variation in $\delta\Theta$ with δI. This is shown in Fig. 6b. Again one sees that $\delta\Theta$ is most stable with respect to changes in δI for $\delta\Theta = \pi/2$ and becomes completely unstable at the edges of the step, $\delta\Theta = 0$ or π. Note that for the range of negative $\delta\Theta$, where the current leads the oscillator phase, $d(\delta\dot{\Theta})/d(\delta\Theta) > 0$; hence, the phase-locked solution is unstable.

5. Phase-Locking in Arrays

5.1. *Locking Strength within the RSJ Model*

A detailed analysis of phase-locking in arrays has been carried out in Jain *et al.* [17], Chapter 6, as well as in Likharev [4], Chapter 13. The discussion presented here in terms of phase-locking to external radiation will, it is hoped, be intuitive while minimizing the mathematical complications. For large arrays, this approach gives nearly the same results as does the more exact analysis. To begin, consider a series array of identical junctions, modeled by their HF equivalent circuits and connected in a loop through a load Z_ℓ as shown in Fig. 7. If all of the oscillators have the same phase, then the rf current that flows in series through all of the junctions and the load is

$$\tilde{I}_\ell = \frac{\tilde{V}_1}{R_J z_c}, \tag{5.1}$$

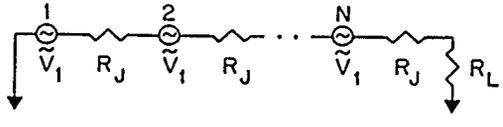

Fig. 7. Equivalent HF circuit for an array terminated in load Z_ℓ.

where the coupling impedance per junction z_c is given in terms of the load impedance Z_ℓ and the junction impedance R_J as

$$z_c = \frac{1}{NR_J}(NR_J + Z_\ell). \tag{5.2}$$

To calculate how much the critical current of one of the junctions can be varied without having it come unlocked from the array, we can just treat this current as external radiation assuming that the array is large enough that a variation of the phase of a single junction will have a negligible effect on $\tilde{I}_\ell$.

When all of the oscillators are running in phase, the relative phase of an oscillator and the locking current is fixed by the loop impedance. Since this impedance always contains a real part equal to the sum of the junctions' resistances plus the load resistance, it is clear that the ideal situation of having the locking current lag the oscillator phase by $\pi/2$ cannot be achieved for the circuit shown in Fig. 7 unless $\mathrm{Im}(Z_\ell) \to \infty$. Thus, in optimizing $\mathrm{Im}(Z_\ell)$ for the maximum locking strength, there is a tradeoff between the amplitude of the locking current and its phase, the phase being given by

$$p_\ell = \tan^{-1}\left[\frac{-\mathrm{Im}(z_c)}{\mathrm{Re}(z_c)}\right]. \tag{5.3}$$

We now wish to see how far the bias current (or critical current) of the kth junction can be varied from the mean for the array without the junction coming unlocked. The mixing current for this junction I_{mk} is

$$I_{mk} = I_L \cos(p_\ell + \delta\Theta_k), \tag{5.4}$$

where $\delta\Theta_k \equiv \bar{\Theta} - \Theta_k$, $\bar{\Theta}$ being the mean phase of the oscillators, and

$$I_L = I_c \frac{\alpha\bar{v}_1}{|z_c|}. \tag{5.5}$$

Note that the product $\alpha\bar{v}_1$ is a maximum near $\bar{v} = 1$, since $\bar{v}_1 \propto \bar{v}$ for $\bar{v} \ll 1$ and $\alpha \propto 1/\bar{v}$ for $\bar{v} \gg 1$.

As for the case of a single junction locked to external radiation, phase-locking will be maintained for $-p_\ell \le \delta\Theta_k \le \pi - p_\ell$. Since $p_\ell \neq \pi/2$, it will be possible to shift I_{ck} farther in one direction than in the other. In a real array, one would likely have a symmetric, roughly gaussian distribution of critical currents with the operating frequency of the array determined by the mean I_c of the distribution. In that case, the maximum width that this distribution could have and still maintain complete locking would be set by the lesser of the

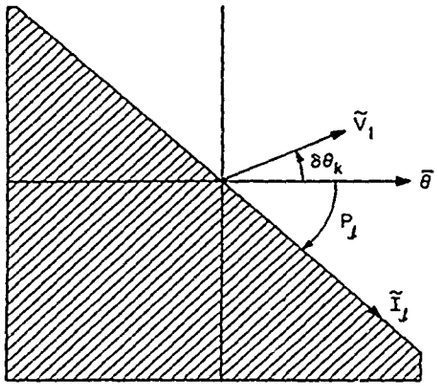

Fig. 8. Relative phase of the mean oscillator voltage (real axis). load current $\tilde{I}_\ell$, and kth junction with different bias or critical current for the array modeled in Fig. 7. Hatched region is unstable.

two deviations, i.e., by

$$\delta I_{k\max} = I_L \min\{1 + \cos p_\ell, 1 - \cos p_\ell\}. \tag{5.6}$$

These phase relations are illustrated in Fig. 8.

Just as with a junction locking to external radiation, the stable situation is when the locking current lags the Josephson oscillator, i.e., the load must be inductive. The inductance that gives the largest locking strength can easily be determined by maximizing Eq. (5.6) with respect to L. If the load impedance is $Z_\ell = R_\ell + jL\omega$, then the locking strength is a maximum for

$$L\omega = \sqrt{3}\,(NR_J + R_\ell), \tag{5.7}$$

so for strong locking, the coupling impedance must have a large reactive component with an inductive character. One can also see the importance of this reactance by calculating the variation in $\delta\Theta_k$ with changes in I_{bk} from Eq. (5.4). Near equilibrium ($\delta\Theta_k = 0$), this variation is

$$\left[\frac{\partial(\delta\Theta_k)}{\partial(\delta I_k)}\right]^{-1} \propto |\tilde{I}_\ell| \sin p_\ell \propto \frac{\sin p_\ell}{|z_c|}, \tag{5.8}$$

i.e., the phase stability is proportional to $\mathrm{Im}(y_c)$, where $y_c = 1/z_c$. Subject to this constraint the maximum power will be delivered to R_ℓ when $R_\ell = NR_J$.

Thus, $L\omega = 2\sqrt{3}\,NR_J$ gives $p_\ell = \pi/3$ and a value for $\delta I_{k\max}$ of

$$\frac{\delta I_{k\max}}{I_c} = \frac{\alpha\bar{v}_1}{8}. \tag{5.9}$$

Using the RSJ values for α and $\bar{v}_1$ with $\bar{v} = 1$ gives

$$\frac{\delta I_{k\max}}{I_c} \approx .04. \tag{5.10}$$

Therefore, the total spread in I_{bk} for this type of array can be about 8% before junctions will start to unlock. Since I_b/I_c is about 1.4 (in the RSJ model) for $\bar{v} = 1$, this implies a permissible variation in I_c of about 10%. This number is a maximum since the spread of I_c for the junctions near the center of the distribution will produce some scatter in their phases with a consequent small reduction in the locking current $\tilde{I}_\ell$.

If we are concerned about the unlocking of the first few junctions in the tails of a large distribution, the estimate above is rather close, as can be shown from computer simulations [21]. It is worth noting that the interaction range of the junctions in this type of array is essentially infinite, i.e., the interaction of the kth and ℓth junctions does not depend on their separation. As a consequence, the unlocking of several junctions in a large array has a negligible effect on the phase-locking among the remaining junctions. It may be undesirable to have even one junction unlocked, however, since if its frequency is close enough to that of the array, mixing will occur, which will modulate the array frequency to some degree. As the width σ of the I_c distribution is increased and additional junctions unlock, $\tilde{I}_\ell$ will begin to decrease, causing yet more junctions to unlock and leading to a rapid uncoupling of the array with increasing σ. Computer simulations on a 40-junction array show that this "catastrophic" failure occurs for a value of σ about twice that at which the junctions in the tail of the distribution first unlock.

We conclude this section with some brief comments on the prospects for two-dimensional linear arrays. As discussed above, when RSJs are connected in an inductive loop, their rf voltage tends to add in-phase around the loop. For the two-dimensional arrays shown in Figs. 4b,c, the lowest impedance path seen by a junction is the inductive path through the junction in parallel with it. For these configurations, the tendency is for the rf polarities to change along a parallel chain of junctions with the result that circulating currents are set up within the chain. Hence, power is dissipated internally instead of being coupled to the load. For the two-dimensional array in Fig. 4d, on the other hand, the lowest impedance path for all of the series chains is the (presumably

inductive) path through the load. Consequently, one would expect a constant phase transverse to the current flow, as desired, for this array. Capacitive coupling between the chains might further stabilize this situation. These stability arguments are developed in much greater detail in Jain *et al.* [17].

5.2. *Radiation Linewidth of Arrays*

Each junction of an array has an intrinsic noise current $S_{I_k}(0)$ that tends to vary the junction's voltage and thus the array's frequency. In the discussions above, we determined the phase-locking effect of the array on a single junction of the array by treating the remaining N-1 junctions as a fixed frequency external source. In this approximation, the frequency of the perturbed junction clearly would not change as long as it remained phase-locked to the array. Thus, no information is provided about the linewidth. The more exact treatment needed to calculate the linewidth is given in Jain *et al.* [17], Chapter 6. Again, one starts from Eq. (4.4). However, the mixing current for the kth junction I_{mk} is now calculated using the rf current obtained by explicitly summing the rf voltage due to all of the other junctions, whose frequencies can now depend on the bias current of the kth junction. Considering an array of N identical junctions as in Fig. 9, this analysis yields an almost intuitive result: Changing the effective low frequency bias current $I_{ek} \equiv I_{bk} + I_{nk} + I_{mk}$ of the kth junction while keeping that of the other N-1 junctions fixed, i.e., $R_s \gg NR_J$, changes the low frequency voltage of the kth junction (and thus the rest of the array since all junctions are phase-locked) by a factor $1/N$ of

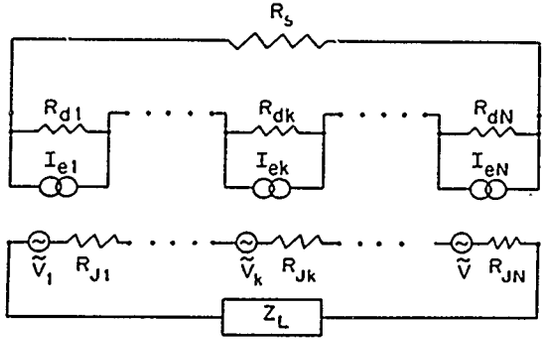

Fig. 9. LF and HF equivalent circuit of junctions coupled in linear array showing LF shunt R_s and HF coupling load Z_L.

that obtained if the junction were not coupled to the array. That is,

$$\delta V_A = \frac{1}{N} R_{dk}\, \delta I_{ck}. \tag{5.11}$$

From Eq. (2.6), $\Delta v \propto R_d^2$, so this reduction of the differential resistance due to phase-locking would narrow the linewidth by a factor N^2. However, there are N noise sources, so their incoherent sum results in an effective noise current with low frequency spectral density $S_I(0) \propto N$, giving for the linewidth Δv_A of the phase-locked array,

$$\Delta v_A = \frac{1}{N} \Delta v_J, \tag{5.12}$$

where Δv_J is the linewidth of a junction when it is not coupled to the array. For example, while a single 0.1 Ω junction would ideally have a linewidth of about 16 MHz, an array of, say, 1000 such junctions should have a 16 kHz linewidth. If the junctions' resistance is varied along with N so that the total array impedance NR_J remains constant, the linewidth would vary as $1/N^2$, e.g., a single 100 Ω junction should have a linewidth of 16 GHz! As we shall see next, even greater reductions in linewidth are possible if the effects of low frequency shunting are taken into account.

Consider the case where the low frequency shunt $R_s \ll NR_d$. Then one can see from Fig. 9 that the noise voltage generated by the junctions' noise currents is largely shorted by R_s giving an intrinsic linewidth Δv_{A_i} of

$$\Delta v_{A_i} \approx \frac{1}{N^3} \Delta v_J \left(\frac{R_s}{R_d}\right)^2. \tag{5.13}$$

If one takes $R_s \approx R_d$, this imples a dramatic linewidth reduction in large arrays—by a factor of N^3! This soon reaches the point where the intrinsic noise will be dominated by coherent noise sources, e.g., by the Johnson noise voltage generated by R_s. Since this voltage is divided equally across all the junctions in a phase-locked array, $S_v(0) \propto 1/N^2$, giving a factor N^2 reduction in linewidth Δv_{A_s} due to the shunt. So,

$$\Delta v_{A_s} \approx \frac{1}{N^2} \Delta v_s, \qquad \Delta v_s \equiv \frac{1}{\pi}\left(\frac{2\pi}{\Phi_0}\right)^2 k_B R_s T_s, \tag{5.14}$$

where T_s is the temperature of the shunt and Δv_s is the linewidth a single junction would have if its voltage noise were that produced by R_s. This is

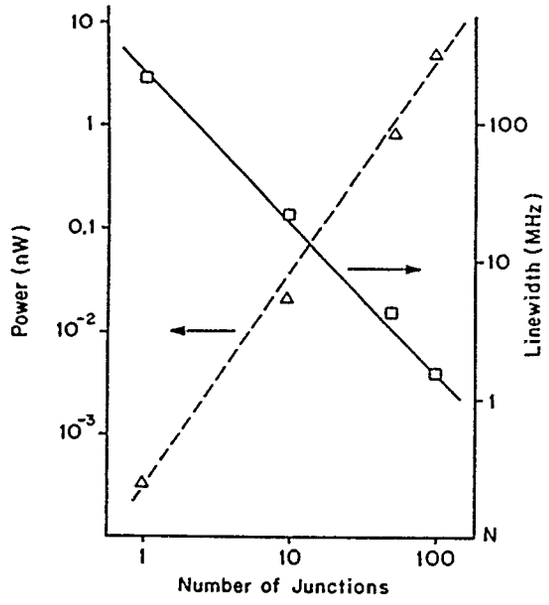

Fig. 10. Power (△) and line width (□) as a function of junction number for a low impedance ($\ll 50\ \Omega$) one-dimensional array of microbridge junctions, with $\nu_0 = 10$ GHz, $Z_L = 50\ \Omega$.

worth noting since it implies that, in large arrays, there may not be a penalty in linewidth for using noisy, e.g., high J_c, junctions.

A possibly severe penalty for the use of low impedance shunts is the large increase in bias and cooling power that they can require. Since, roughly speaking, only noise up to frequencies $\Delta\nu$ contributes to $\Delta\nu$, a shunt in a large array must only be effective at very low frequencies. A rather large inductance should thus be tolerable in series with the shunt resistor, making it possible to place this resistor, for example, at 77 K. While this would increase the linewidth due to the shunt, this linewidth would still be so small as to be acceptable for most applications.

Experimental evidence for the predicted dependence of power and linewidth on array size is shown in Fig. 10 taken from the result Jain *et al.* [17]. Here arrays of 0.1 Ω microbridge junctions incorporated in a 50 Ω microstrip were measured. The power is seen to increase as N^2 as is expected for the coherent state of this array, since the array impedance is always much less than that of the load (see Section 2). Since the low frequency shunting in this array is negligible, the linewidth is expected to vary as $1/N$ as observed.

5.3. *Effects of Capacitance on Phase-Locking in Arrays*

So far only junctions with no capacitance have been considered. In this section, we will examine what changes in the behavior of arrays one might expect if $\beta_c \neq 0$. One must be aware that capacitance is dangerous. A clue to this is seen in the locking of a single junction to external radiation where the situation corresponding to a capacitive load, i.e., the current phase leading the oscillator, is unstable. It has been shown that for an array like that in Fig. 7, the uniform phase solution is unstable if Z_ℓ is capacitive [17,4]. Instead, the rf voltage tends to sum to zero around the loop. Further, there are many examples of chaotic behavior in capacitive junctions subject to applied radiation or external loads. In spite of this, there are several reasons to consider using capacitive junctions in arrays.

Potential advantages of capacitive junctions are the following: By far the most advanced technology for making Josephson junctions is for tunnel junctions where capacitance is unavoidable. Also, as we shall see below, the presence of a small shunt capacitance can, under certain conditions, enhance the locking strength in the array. Indeed, there have been very successful examples of locking large arrays of high capacitance tunnel junctions to external radiation [6], as well as demonstrations that even junctions with $\beta_c \gg 1$ can phase lock and generate radiation [22–26,13]. Furthermore, it has been shown that tunnel junctions generate significant power levels, at least up to the sum of the gap frequencies [27]. Fortunately, a very general technique for analyzing the stability of the uniform solution in arrays with arbitrary β_c and Z_ℓ has been developed by Hadley *et al.* [28,29]. This should be of great help in designing arrays of capacitive junctions to avoid the "dangerous" regions of parameter space.

In this section, the analysis above for arrays of junctions with $C = 0$ will be extended, using perturbation theory, to the case of small C, i.e., for $\beta_c \leq 1$, in order to develop some insight into the effects of capacitance. This low C region near $\bar{v} \geq 1$, where one can still hope to obtain meaningful results from perturbation theory, is also the region in which the analysis of Hadley *et al.* [28,29] indicates that the uniform solution should have the greatest stability.

In order to include the effects of junction capacitance, a capacitor will be connected across the HF terminals of the junction and treated as an additional perturbation. The details of this analysis, which is summarized below, are shown more completely in Lukens *et al.* [3]. The effects of the various perturbations to the junction are additive since the circuits are linear. The direct effect of the shunt capacitor on the junction will be to change the voltage

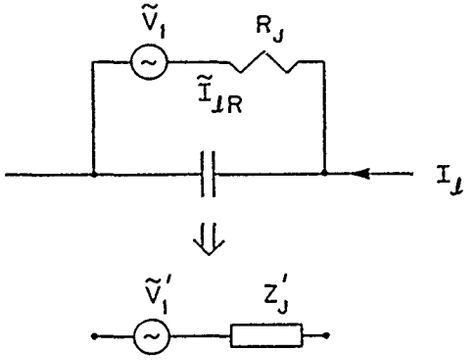

Fig. 11. (a) HF equivalent circuit of a junction with a capacitor for perturbation. (b) Equivalent circuit as seen by the rest of the array.

$\bar{V}$ obtained for a given bias current. This will be ignored since to first order it does not influence the locking behavior of the junction, but just means that a slightly different bias must be used to achieve the desired frequency. The most important effects of the capacitance are to change the effective impedance and rf voltage of the junction as seen by the rest of the circuit. This is illustrated in Fig. 11.

These junctions are now connected in a loop in series with a resistive load having a resistance, in units of NR_J, of r_ℓ. The phase shift between the junctions' oscillators and the loop current $\tilde{I}_\ell$ produced by the shunt capacitance is

$$p_\ell = \tan^{-1}\left(\frac{-\beta_c \bar{v} r_\ell}{r_\ell + 1}\right),$$

which has the same sign as that due to an inductance in series with the load. Thus, the phase relationship between the loop current and the oscillators is that required for stable locking, even with a purely resistive load. The fraction of $\tilde{I}_\ell$ that flows through R_J, $\tilde{I}_{\ell R}$, is responsible for the phase-locking. $\tilde{I}_{\ell R}$ is further shifted with respect to $\tilde{I}_\ell$ by a phase $\tan^{-1}(-\beta_c \bar{v})$ giving a total phase shift $p_{\ell R}$ between the oscillators and $\tilde{I}_{\ell R}$ that can exceed $\pi/2$. These phase relations are illustrated in Fig. 12 and show a potential advantage of the shunt capacitance over a series inductance. Recall from Section 5.1 that the locking strength and hence the acceptable scatter in I_c was substantially reduced with an inductance, since it was not possible to have a $\pi/2$ phase shift between the mean phase of oscillators and the locking current. With a shunt capacitance

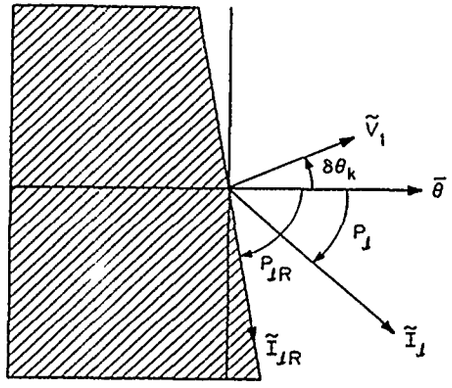

Fig. 12. Relative phases of the oscillators, loop current $\tilde{I}_\ell$, and locking current $\tilde{I}_{\ell R}$ for an array of capacitive junctions.

one can achieve this optimum phase shift by choosing

$$\beta_c \bar{v} = \left(\frac{1 + r_\ell}{r_\ell}\right)^{1/2}.$$

There is a large parameter space in $\bar{v}$, β_c and Z_ℓ that can be explored to optimize the power and locking strength for a given application. To get a feel for the performance of these arrays with $\beta_c > 0$, let us take the purely resistive load that maximizes the load power for given β_c and $\bar{v}$. This gives

$$r_\ell = [1 + (\beta_c \bar{v})^2]^{-1/2}. \tag{5.15}$$

The desired $\pi/2$ phase shift is then obtained for $\beta_c \bar{v} = \sqrt{3}$. For these values the locking strength is

$$\frac{\delta I_k}{I_c} = \frac{\alpha \tilde{v}_1}{2\sqrt{3}}. \tag{5.16}$$

This is more than twice that for the RSJ array from Eq. (5.9), indicating that complete locking should still be possible with a total spread in I_c of greater than 20%. For smaller values of $\bar{v}$, the limits of perturbation theory are being pushed, so the exact values need to be compared with computer simulations. We note that the estimate from perturbation theory is in line with the result of simulations done by Hadley *et al.* [28,29] on 100-junction arrays with $\beta_c \approx 0.75$ and $i \approx 2.3$, where locking was still observed with a scatter greater than 15% in R_J, C, and I_c.

6. Distributed Arrays

In all of the discussions above, it has been assumed that the dimensions of the arrays were much less than the wavelength λ. As a result, the lumped circuit approximation could be used. To see if this is realistic, note that if the entire array is to have a length less than $\lambda/8$ the junction spacings must be

$$s = \frac{1}{8}\frac{v_p}{\nu N} \approx 0.1\ \mu\text{m}, \tag{6.1}$$

where $v_p \approx 10^8$ m/s is the propagation velocity in the superconducting transmission line connecting the junctions, and the value of νN from Eq. (3.1) has been used. Unfortunately, 0.1 μm spacing is about two orders of magnitude closer than is practical to place the junctions in the array when such things as heating and the limits of lithography are considered. We conclude that in order to achieve maximum power, even from one-dimensional arrays, the junctions must be distributed over a wavelength or more.

The analysis of phase-locking above has shown that the phase of the junctions' oscillations relative to the locking current flowing in the coupling circuit is crucial. In general, an oscillator in a transmission line will generate waves propagating in both directions. This makes it impossible to maintain the same phase relationship between all of the oscillators and the locking current when the junctions are placed at arbitrary positions along the transmission line. There have been several proposals [17,30,31] for placing junctions along a transmission line such that they will phase-lock. The simplest approach, described in this section, is just to place the junctions at wavelength intervals along the transmission line. Hence, all junctions see the same impedance and the same relative phase. The analysis of this circuit at the frequency ν_λ, where the spacing is equal to λ, is identical to the lumped circuit analysis above. The disadvantage of this approach is that it is only valid at a discrete set of frequencies. It is therefore not clear that such an array will be continuously tunable over a large range of frequencies.

Figure 13 shows a schematic of such a distributed array. The junctions are placed at λ intervals along a serpentine microstrip transmission line. An independently biased detector junction is placed immediately after a load resistor in the line. By measuring the range of detector bias current over which the detector phase locks to the array-generated locking current flowing through the load resistor, the power to the load can be determined for each operating frequency of the array. The ends of the array are terminated with $\lambda/4$ stubs so that, to the junctions, the array appears grounded through the

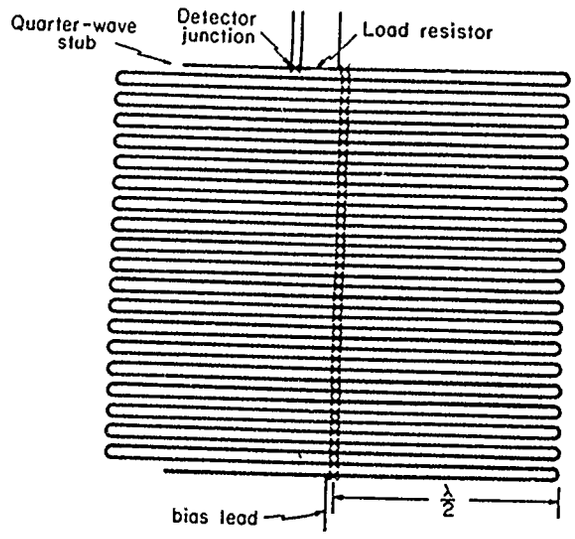

Fig. 13. Layout of distributed array. Oscillator junctions (×) are placed at wavelength intervals along the serpentine microstrip. Load resistor and detector junction to monitor the load current are shown at upper left.

load resistor. Additional length can be added to the stub in order to add a reactive component to the load to optimize the locking strength.

The current amplitude of the Josephson step in the detector junction of such an array is shown in Fig. 14 as a function of the average frequency of the array junctions as determined by measuring the dc voltage across the array [32]. This array contained 40 junctions, which were biased in series, with the bias current flowing through the microstrip. The junctions were separated by 1 mm of microstrip giving an expected value for ν_λ of 100 GHz. Indeed a sharp peak in rf current I_ℓ through the detector is observed at 108 GHz indicating the presence of phase-locking near this frequency. The peak value of the rf current, however, is that expected if only seven of the forty junctions were locked in-phase. It is possible to directly measure the distribution of critical currents of the junctions in the array; the resulting distribution is in fact too broad for complete locking. From the measured maximum rf current and the distribution of I_c's, one concludes that only seven or eight of the junctions could be phase-locked. Thus, the data show that the junctions that are sufficiently uniform to lock lock with very nearly the same phase, as predicted.

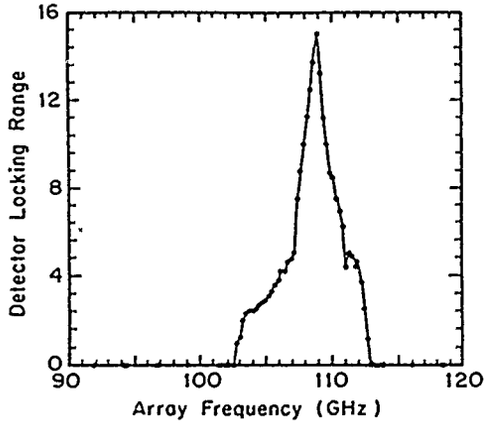

Fig. 14. RF current in transmission line (as measured by detector locking range) vs. average frequency junctions in array.

Since our fabrication process does not yield sufficiently uniform critical currents to insure that locking would be achieved if all junctions were biased with the same current, a "parallel" bias scheme has been used. The superconducting bias leads inject (remove) current at alternate bends in the microstrip, as seen in Fig. 15, with the result that each junction is part of two interlocking dc SQUIDS. All junctions then have the same average voltage, which alternates in polarity along the microstrip. This forces the bias current to divide so as to compensate to first order for the variations in the junctions' critical currents. The rf locking current is still crucial, however, since without it the phase of each junction would be essentially random due to random flux linking the SQUIDs. Further, noise currents would cause voltage (and frequency) fluctuations among the junctions. Phase-locking for this type of parallel biasing has been analyzed in detail in Jain *et al.* [17]. It is primarily as discussed above for series-biased junctions except that the effective scatter in I_c approximately equals Φ_0/L, where L is the inductance of the dc SQUID. For this circuit $\delta I_c \approx 5\mu A$. The junctions are resistively shunted Pb-alloy tunnel junctions having an area of about 1.5 μm^2. These resistively shunted junctions, which have $I_c = 2.5$ mA, have been described in detail elsewhere [31].

The junctions' separation in this array is 350 μm giving a value for ν_λ of 350 GHz. The power (as determined from the rf current through the detector and the 23 Ω load resistor) vs. frequency is shown in Fig. 16. Significant power is observed starting at about ν_λ; however, the array also generates over 1 μW of

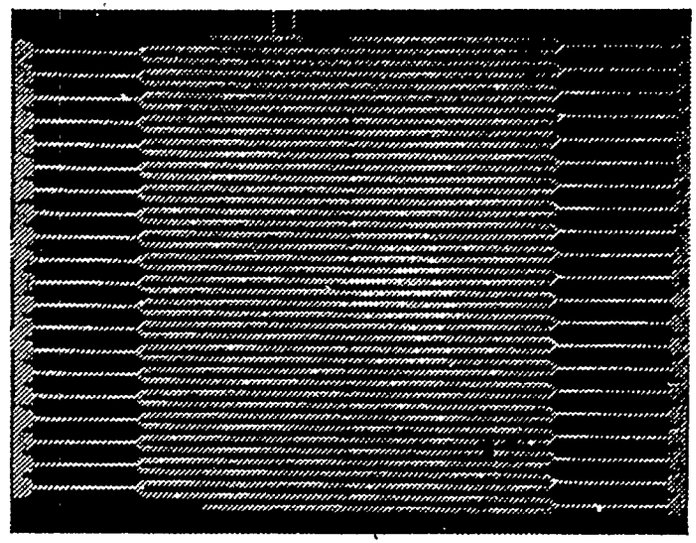

(a)

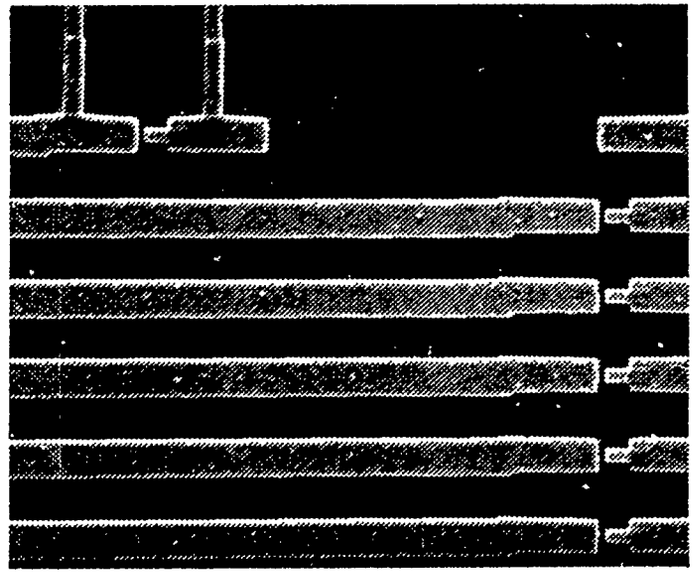

(b)

Fig. 15. (a) Micrograph of distributed array. (b) Blowup of (a), top left, showing detector junction, load resistor, and several oscillator junctions on the right. The vertical separation of the oscillators is 10 μm.

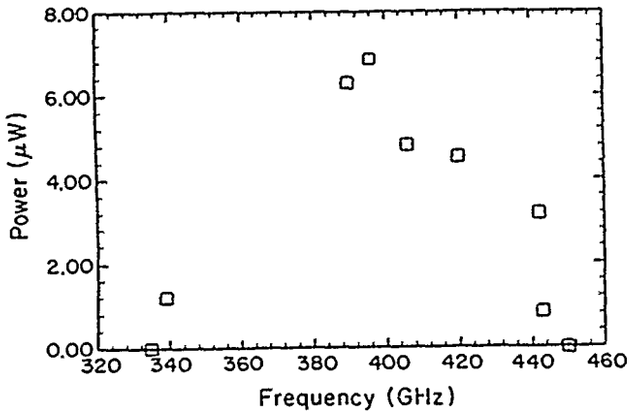

Fig. 16. Power delivered to 23 Ω load resistor vs. array frequency for 40-junction array. Junction parameters: $I_c = 2.5$ mA and $R = 0.5\ \Omega$.

power at a number of discrete frequencies over a band from 340 GHz to 440 GHz, where the junctions are not separated by integer wavelengths. The maximum power of 7 μW is consistent with all 40 junctions of the array locked in-phase. Other arrays with lower critical current junctions are continuously tunable through this band delivering more than 1 μW of power [33,34], again consistent with all junctions in-phase.

7. Prospects for the Future

As of this writing, the distributed arrays described above are the most powerful fundamental solid state sources at 400 GHz. Rather straightforward, though technically complex, extensions of that work should result in sources operating at over 1 THz with nearly 1 mW of power. Clearly, much work—both experimental and theoretical—needs to be done. This is especially true when considering wide ($w \approx \lambda_{em}/2$) junctions and two-dimensional arrays, where there are essentially no experimental results at present. Probably the most immediate problem is to couple the submillimeter radiation off-chip to determine its spectral purity. Fortunately, very broadband antennas have recently been demonstrated in this frequency range [35,36] for use with superconducting SIS mixers. Also, more theoretical work is needed to understand the unexpectedly wide tuning range seen in many of the distributed arrays.

Table 1. Prospective Sources at 1 Terahertz[a]

Array dimension	1	1	2
Junction (array) width	$2\lambda_J$ ($2\lambda_J$)	$\lambda_{em}/2$ ($\lambda_{em}/2$)	$\lambda_{em}/2$ ($\lambda_m/2$)
J_c [A/cm^2]	—	2×10^6	2×10^6
I_c [mA]	4	40	40
Number of junctions	100	1000	10^6
Power [mW]	0.1	10	10^3
Linewidth (no LF shunt)	5 MHz	50 kHz	50 Hz
Linewidth (1 Ω LF shunt)	20 kHz	200 Hz	< 1 Hz

[a] Estimates are based on parameters for nonhysteretic NbAlNb junctions with effective length $2\lambda_J$. A 50 Ω load is assumed. λ_t is the wavelength in the transmission line.

Table 1 summarizes the range of powers and linewidths that might be expected from several different types of arrays, based on the discussions in this chapter. These range from one-dimensional, unshunted arrays of narrow junctions in the upper left of the table, to two-dimensional, linear arrays of the type shown in Fig. 4c with low frequency shunts, at the lower right. Essentially, the projections in the upper left are rather straightforward extrapolations of present design, while, moving to the lower right, one ventures into a territory with progressively more ideas that have yet to be tested. It would, for example, be surprising if a 1 Hz linewidth at one terahertz were ever achieved.

Finally, it is worth considering what impact the new copper oxide superconductors (HTS) might have on the development of these array sources. The most straightforward application of these materials could be as superconducting ground planes and transmission lines. For a given type of conventional superconductor, e.g., niobium, transmission lines become very lossy at half of the upper frequency limit for the junctions' oscillation. Thus, the upper frequency limit might be doubled using HTS microstrip, e.g., to about 3 THz using NbN junctions. While making high quality tunnel junctions of HTS material may be some time in the future, it is worth remembering that the array oscillators do not require good tunneling characteristics. Junctions, e.g., microbridges, with a normal metal barrier should work well; preliminary reports of such thin film junctions which show the Josephson effect have already been presented [37]. While the use of HTS junctions may well extend the upper frequency limit of Josephson effect sources to above 10 THz, the most important advantage initially should be to permit operation at 77 K and thus enhance compatibility with many semiconductor systems. From all of this, we see that Josephson sources have a great, perhaps unique, potential for filling a real void throughout the submillimeter wave band.

Acknowledgments

I would like to acknowledge the essential contributions of all those at Stony Brook who have worked so hard over the years on the development of array sources and especially to thank A.K. Jain, K.-L. Wan, and J.E. Sauvageau, whose work on distributed arrays pushed Josephson sources into the realm of respectability. Special thanks is also due to K.K. Likharev for his valuable and stimulating contributions to our understanding of arrays made during his summer at Stony Brook. Various aspects of the work on arrays at Stony Brook have been supported at different times by the Office of Naval Research, the Air Force Office of Scientific Research, and the Strategic Defense Initiative through the Air Force terahertz technology program.

References

1. Tsai, J.S., Jain, A.K., and Lukens, J.E. High-precision test of the universality of the Josephson voltage-frequency relation. *Phys. Rev. Lett.* **51**, 316–319 (1983).
2. Jain, A.K., Lukens, J.E., and Tsai, J.-S. Test for relativistic gravitational effects on charged particles. *Phys. Rev. Lett.* **58**, 1165–1168 (1987).
3. Lukens, J.E., Jain, A. K., and Wan, K.-L. Application of Josephson effect arrays for submillimeter sources. *In* "Proceedings of the NATO Advanced Study Institute on Superconducting Electronics" (M. Nisenoff and H. Weinstock, eds.). Springer-Verlag, Heidelberg, to be published, 1989.
4. Likharev, K.K. "Dynamics of Josephson Junctions and Circuits." Gordon and Breach, New York, 1986.
5. Basovaish, S., and Broom, R.F. Characteristics of in-line Josephson tunneling gates. *IEEE Trans. Magn.* **11**, 759–762 (1975).
6. Kautz, R.L., Hamilton, C.A., and Lloyd, F.L. Series-array Josephson voltage standards. *IEEE Trans. Magn.* **23**, 883–890 (1987).
7. Yoshida, K., Qin, J., Enpuku, K. Inductive coupling of a flux-flow type Josephson oscillator to a stripline. *IEEE Trans. Magn.* **25**, 1084–1087 (1989).
8. Nagatsuma, T., Enpuku, K., Irie, F., and Yoshida, K. Flux-flow-type Josephson oscillator for millimeter and submillimeter wave region. *J. Appl. Phys.* **54**, 3302–3309 (1983).
9. Cirillo, M., Modena, I., Carelli, P., and Foglietti, V. Millimeter wave generation by fluxon oscillations in a Josephson junction. *J. Appl. Phys.*, to be published (1989).
10. Monaco, R., Pagano, S., and Costabile, G. Superradiant emission from an array of long Josephson junctions. *Phys. Lett. A* **131**, 122–124 (1988).
11. Pagano, S., Monaco, R., and Costabile, G. Microwave oscillator using arrays of long Josephson junctions. *IEEE Trans. Magn.* **25**, 1080–1083 (1989).
12. Likharev, K.K., and Semenov, V.K. Fluctuation spectrum in superconducting point junctions. *JETP Lett.* **15**, 442–445 (1972). Reprinted from *2hETF Pis. Red.* **15**, No. 10, 625–629.
13. Smith, A.D., Sandell, R.D., Silver, A.H., and Burch, J.F. Chaos and bifurcation in

Josephson voltage-controlled oscillators. *IEEE Trans. Magn.* **23**, 1267–1270 (1987).
14. Clark, T.D. Experiments on coupled Josephson junctions. *Phys. Lett. A* **27**, 585–586 (1968).
15. Tilley, D.R. Superradiance in arrays of superconducting weak links. *Phys. Lett. A* **33**, 205–206 (1970).
16. Clark, T.D. Electromagnetic properties of point-contact Josephson junction arrays. *Phys. Rev. B* **8**, 137–162 (1973).
17. Jain, A.K., Likharev, K.K., Lukens, J.E., and Sauvageau, J.E. Mutual phase-locking in Josephson junction arrays. *Phys. Rep.* **109**, 309–426 (1984).
18. Lindelof, P.E., and Hansen, J.B. Static and dynamic interactions between Josephson junctions. *Rev. Mod. Phys.* **56**, 431–459 (1984).
19. Forder, P.W. A useful simplification of the resistively shunted junction model of a Josephson weak-link. *J. Phys. D* **10**, 1413–1436 (1977).
20. Kuzmin, L.S., Likharev, K.K., and Ovsyannikov, G.A. Mutual synchronization of Josephson contacts. *Radio Eng. & Electron. Phys.* **26**, No. 5, 102–110 (1981).
21. Sauvageau, J.E. Phase-locking in distributed arrays of Josephson junctions. Ph.D. dissertation, State University of New York at Stony Brook, 1987.
22. Finnegan, T.F., and Wahlsten, S. Observation of coherent microwave radiation emitted by coupled Josephson junctions. *Appl. Phys. Lett.* **21**, 541–544 (1972).
23. Lee, G.S., and Schwarz, S.E. (1984). Numerical and analytical studies of mutual locking of Josephson tunnel junctions. *J. Appl. Phys.* **55**, 1035–1043 (1984).
24. Lee, G.S., and Schwarz, S.E. Mutual phase locking in series arrays of Josephson tunnel junctions at millimeter-wave frequencies. *J. Appl. Phys.* **60**, 465–468 (1986).
25. Kuzmin, L.S., Likharev, K.K., and Soldatov, E.S. Experimental study of mutual phase locking in Josephson tunnel junctions. *IEEE Trans. Magn.* **23**, 1051–1053 (1987).
26. Krech, V.W., and Reidel, M. Synchronisationseffekte in Anordnungen aus zwei Josephson Verbindungen mit endlichem McCumber-Parameter. *Ann. Phys. (Leipzig)* **44**, 329–339 (1987).
27. Robertazzi, R.P., and Buhrman, R.A. NbN Josephson tunnel junctions for terahertz local oscillators. *Appl. Phys. Lett.* **24**, 2441–2443 (1988).
28. Hadley, P., Beasley, M.R., and Wiesenfeld, K. Phase-locking of Josephson junction arrays. *Appl. Phys. Lett.* **52**, 1619–1621 (1988).
29. Hadley, P., Beasley, M.R., and Wiesenfeld, K. Phase-locking of Josephson junction series arrays. *Phys. Rev. B* **38**, 8712–8719 (1988).
30. Davidson, A. New wave phenomena in series Josephson junctions. *IEEE Trans. Magn.* **17**, 103–106 (1981).
31. Sauvageau, J.E., Jain, A.K., Lukens, J.E., and Ono, R.H. Phase-locking in distributed arrays of Josephson oscillators. *IEEE Trans. Magn.* **23**, 1048–1050 (1987).
32. Sauvageau, J.E., Jain, A.K., and Lukens, J.E. Millimeter wave phase-locking in distributed Josephson arrays. *Int. J. of Infrared & Millimeter Waves* **8**, 1281–1286 (1987).

33. Wan, K.-L., Jain, A.K., and Lukens, J.E. Submillimeter wave generation using Josephson junction arrays. *IEEE Trans. Magn.* 25, 1076–1079 (1989).
34. Wan, K.-L., Jain, A.K., and Lukens, J.E. Submillimeter wave generation using Josephson junction arrays. *Appl. Phys. Lett.*, to be published (1989).
35. Büttenbach, T.H., Miller, R.E., Wengler, M.J., Watson, D.M., and Phillips, T.G. A broad-band low-noise SIS receiver for submillimeter astronomy. *IEEE Trans. Microwave Theory Tech.* 36, 1720–1726 (1988).
36. Li, X., Richards, P.L., and Lloyd, F.L. SIS quasiparticle mixers with bow tie antennas. *Int. J. Infrared & Millimeter Waves* 9, 101–133 (1988).
37. Schwartz, D.B., Mankiewich, P.M., Howard, R.E., Jackel, L.D., Straughn, B.L., Burkhardt, E.G., and Dayem, A.H. The observation of the ac Josephson effect in a $YBa_2Cu_3O/Au/YBa_2Cu_3O_7$ junction. *IEEE Trans. Magn.* 25, 1298–1300 (1989).

VOLUME 58, NUMBER 12 PHYSICAL REVIEW LETTERS 23 MARCH 1987

Test for Relativistic Gravitational Effects on Charged Particles

A. K. Jain, J. E. Lukens, and J.-S. Tsai[(a)]

Department of Physics, State University of New York, Stony Brook, New York 11794

(Received 14 November 1986)

Experimental results are presented which provide the first measurement of the effects of a gravitational field on charged particles, equivalent to the red shift for photons. Two Josephson-effect batteries ($V \simeq 300$ μV) having a vertical separation of 7.2 cm are connected in opposition by superconducting wires. A voltage difference of 2.35×10^{-21} V is maintained between these batteries by means of the gravitational red shift. The emf around this loop is, however, measured to be less than 1×10^{-22} V, consistent with the predicted invariance of the gravito-electrochemical potential along the wires.

PACS numbers: 04.80.+z, 74.50.+r

The strong equivalence principle, which states that locally the effects of a uniform gravitational field are indistinguishable from those due to an accelerating reference frame, is a fundamental postulate of general relativity. A consequence of this equivalence, along with special relativity, is that the rates of identical clocks running in different gravitational potentials will differ. This variation in clock rates implies the gravitational red shift of photons, which was first observed by Pound and Rebka[1] and has, during the past two decades, been verified by a number of workers[2] to a present accuracy of better than 1 part in 10^4. There have, however, previously been no experimental tests of the corresponding effects for charged particles.

One such effect occurs for the conduction electrons in a metal, such as a superconductor, in a gravitational field where, in equilibrium, the electrochemical potential μ will in general not be constant. Rather, a related quantity $\tilde{\mu} = \mu(1+\lambda)$ called the gravito-electrochemical potential will be constant along the wire.[3-6] Here $\lambda = zg/c^2$ and depends on the gravitational potential through the height z; g is the gravitational acceleration at the earth's surface and c the speed of light in a vacuum, giving $\lambda/z = 1.09 \times 10^{-16}$/m. For a resistanceless metal such as a superconductor, $\tilde{\mu}$ should also be independent of position even with a dc current flowing.[6] Thus a circuit with two identical batteries (as measured by local observers) of emf V, separated in height by z and connected in opposition by superconducting wires, would have a net emf $\Delta V = \lambda V$ around the zero-resistance loop leading to a loop current increasing linearly in time.[4]

Within a single wire a purely Newtonian gravitational field can produce a number of effects which shift the electrochemical potential. For instance, the gravitational force on the electrons must be balanced by an electrostatic force giving rise to an electric field (the Schiff-Barnhill field[7]). This latter effect is in fact contained in the potential $\tilde{\mu}$ if the electron rest mass is included, since $\lambda mc^2 = mgz$. An electric field can also be produced because of the shift in the Fermi level induced by lattice distortion due to the gravitational force on the ions.[8] These gravitational effects can be 10 to 15 orders of magnitude greater[9] than the relativistic shift in potential difference discussed above. However, they do not contribute to the net emf around a loop.

In this Letter we report the results[10] of a null experiment to compare the fractional change with height of the electrochemical potential difference between two superconducting wires to the fractional change in photon frequency over the same height, which is given by $\Delta\nu/\nu = \lambda$. The schematic of the experiment is shown in Fig. 1. The "batteries" used to provide the highly precise reference emf's are Josephson junctions separated vertically by a height $z = 7.2$ cm and phase locked to a common external microwave source. The relation between the frequency ν of the external radiation and the dc electrochemical potential difference across the junction, $V \equiv \Delta\mu$, is given by the Josephson equation as

$$V = n\nu\Phi_0, \tag{1}$$

where the integer n is the order of the radiation-induced step in the junction I-V curve. Since the radiation reaching the upper junction is red shifted with respect to

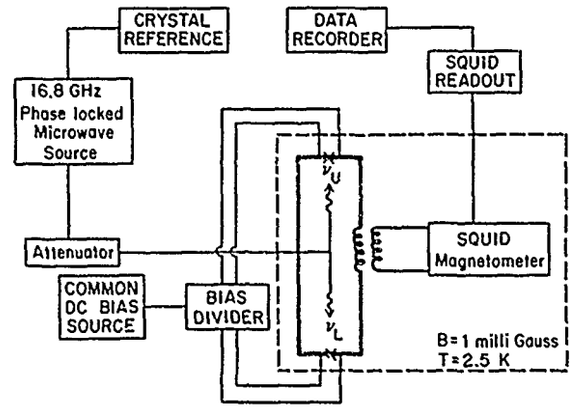

FIG. 1. Schematic of the measurement circuit. The crosses denote the Josephson batteries. The darker lines indicate superconducting portions of the circuit.

© 1987 The American Physical Society

that reaching the lower junction, the potential differences across the upper and lower junctions, V_u and V_l respectively, will differ slightly so that

$$V_u = V_l(1-\lambda). \tag{2}$$

In the absence of additional relativistic effects on the Cooper pairs, one would thus expect the net emf ΔV in the loop containing the junctions to be $\lambda V \simeq 2\times10^{-21}$ V, since $V \simeq 300$ μV and $\lambda \simeq 7\times10^{-18}$ for this experiment. Such a nonzero value for ΔV would lead, as discussed below, to a time-varying flux through the loop. This could be detected by use of a superconducting quantum interference device (SQUID) magnetometer, as shown in Fig. 1. The relativistic prediction that $\bar{\mu}$ =const in the superconducting leads, however, implies that the potential difference V between the leads varies with height so that $V(z) = V(0)(1-\lambda_q)$. The symbol λ_q, which in theory equals λ, has been introduced to allow for the possibility of corrections to the predicted relativistic effects on charged particles. The loop emf is thus $\Delta V = V_l \times(\lambda-\lambda_q)$ and is predicted to be zero on the basis of the strong equivalence principle.

The basic technique for the detection of extremely small voltage differences between two Josephson junctions by monitoring of the flux change in a superconducting loop was developed[11] shortly after the discovery of the Josephson effect. The apparatus used for these measurements is a refined version of that previously used by us to demonstrate the universality of Eq. (1) for different types of Josephson junctions[12] to 2 parts in 10^{16}. The Josephson junctions used here are lead-alloy tunnel junctions with critical currents of $I_c \simeq 900$ μA. The junctions are shunted with low-inductance 0.5-Ω resistors to ensure nonhysteretic operation and have I-V characteristics that are extremely close to those predicted for ideal resistively shunted junctions (RSJ model). The junctions and superconducting leads connecting them are placed over a niobium ground plane giving a total loop inductance of $L \simeq 1$ nH, associated primarily with the coupling inductor to the magnetometer. The microwave radiation is coupled to the junctions by our placing each junction at the end of a capacitively grounded microstrip which is in turn coupled to a coaxial cable through a small section of coplanar waveguide. In order to minimize any extraneous shifts in the relative phases of the radiation reaching the two junctions, these two coaxial cables are connected, just outside the sample cell and halfway between the junctions, to a common cable leading out of the cryostat.

In general Josephson junctions will phase lock to applied radiation over a range of bias current $\Delta I_i = J_i \sin(\delta_i - \pi/2)$, where the maximum current variation—or locking range—is dependent on microwave power. Here, $\delta_i \equiv \theta_i - n\omega_i t$ ($\omega_i = 2\pi\nu_i$) is the difference between the linear component θ_i of the phase of the Josephson oscillations in the ith junction and the phase of the applied radiation at the junction.[13] At a constant gravitational potential the time-averaged fluxoid quantization condition for the loop of inductance L as shown in Fig. 1 is then[14]

$$(\Phi_0/2\pi)(\theta_2-\theta_1) + LI_l + \Phi_a = m\Phi_0, \tag{3}$$

where Φ_a is the flux applied to the loop and $I_l = (\Delta I_2 - \Delta I_1)/2$. For simplicity, identical junctions and locking ranges for 1 and 2 have been assumed.

The emf which drives the changes in the loop current I_l is, from Eq. (3),

$$\frac{\Phi_0}{2\pi}\frac{d}{dt}(\delta_2-\delta_1) + \frac{\Phi_0}{2\pi}n\Delta\omega + \frac{d\Phi_a}{dt},$$

where $\Delta\omega \equiv \omega_2 - \omega_1$. For the SQUID's used in these measurements $\beta_l' \equiv 2\pi LJ/\Phi_0 \gg 1$, thus the terms in δ can be neglected, giving

$$-L\frac{dI_l}{dt} \simeq \frac{d\Phi_a}{dt} + \frac{\Phi_0}{2\pi}n\Delta\omega.$$

The response of this phase-locked system to a small frequency difference $\Delta\omega$, as described by Eq. (3), is the same as the response to an applied flux varying linearly with time for the system biased below the junction critical current in the absence of radiation. For example, if Φ_a is changed (or $\Delta\omega \neq 0$), a loop current will be induced. As long as $I_l < J$, m will remain constant and I_l will increase (nearly) linearly with Φ_a (or time) until $I_l \simeq J$, then m will change and I_l will decay in steps of approximately Φ_0/L as flux quanta enter the loop. In the linear region, for $I_l \ll J$, the rate of change in the loop current is related to $\Delta\omega$ (for constant Φ_a) by

$$-L\frac{dI_l}{dt}l \simeq \Delta V \simeq \frac{\Delta\omega}{\omega}V \tag{4}$$

with the junction voltage $V = n\nu\Phi_0$.

It is important to note from this discussion that, within the constraint of fluxoid quantization, it is possible for the two junctions to have slightly different average voltages while in a fixed fluxoid state, phase locked to the applied radiation. This result, contained in Eq. (4), has previously been demonstrated with a modified version of the apparatus in which separate coaxial cables extended from each junction to outside the cryostat.[12] This permitted the creation of a small frequency difference by Doppler shifting of the radiation going to one of the junctions and served to demonstrate that the sensitivity of the apparatus is indeed correctly predicted by Eq. (4).

The sensitivity limit of the apparatus at a loop emf of 1×10^{-22} V over a typical 10-h run implies that the change in the loop flux Φ due to any extraneous sources must be less than $2\times10^{-4}\Phi_0/\text{h}$. To provide shielding against such small changes in the ambient flux Φ_a, Mu-metal shielding was used to reduce the ambient field to about 1 mG. To stabilize the remaining flux the superconducting loop was enclosed in a superconducting NbTi

box which was placed inside a large lead can. The temperature of the box was regulated to $\pm 50\ \mu$K to prevent thermally induced flux motion. In addition both junctions were fabricated on sapphire substrates to minimize any thermal gradients across the junction and prevent a thermoelectric current from being induced in the loop. Deliberate temperature shifts of 1 mK caused changes in Φ of less than of $1\times10^{-4}\Phi_0$ even during temperature transients.

Additional factors which could cause ΔI_1 or ΔI_2 to change and generate a loop current I_l are changes in the microwave power or frequency or in the junction bias currents I_i. Since there are common sources of microwave and bias current for both junctions, the changes mentioned above, except for the gravitational red shift in frequency, will affect the junctions equally. For identical junctions these extraneous effects would then produce equal changes in ΔI_1 and ΔI_2 causing no change in I_l. Even with the small asymmetries present in the actual apparatus, it has proven possible—as detailed below—to reduce the effects of variations in the bias current and microwave sources to negligible levels.

Current from the common dc bias source was divided between the junctions so that to first order a change in the source current produced no change in I_l. The drift in the current source of 1 part in 10^4 during a run corresponded to an apparent voltage of about 10^{-23} V. The frequency drift of the microwave source, which was phase locked to a quartz-crystal oscillator, was 1 kHz/d. This resulted in a coherent drift in the voltages of the two Josephson batteries of about a picovolt over the course of the measurement. However, the symmetric configuration, with equal microwave path lengths to the two junctions, reduced the flux change through the loop because of this coherent drift to a rate of $4.2\times10^{-5}\Phi_0$/d, corresponding to an apparent loop emf of less than 10^{-24} V. The power output of the microwave source was regulated to about 2 parts in 10^3 by use of a leveling loop. However, the power reaching the junctions varied by about 1.5% during the measurement because of a change in the attenuation of the coaxial cable as the helium level in the cryostat dropped. This variation, which was the largest source of sample-related flux drift, produced an estimated change in Φ of $5\times10^{-4}\Phi_0$ over 12 h to give an apparent loop emf of 0.4×10^{-22} V.

The loop flux was monitored for continuous 10-h periods with use of a commercial rf SQUID magnetometer located in the helium bath. The magnetometer output Φ_m (referred to the sample loop) versus time is shown in Fig. 2, curve *a*, for the loop junctions phase locked on their ninth-order steps to 16.8-GHz radiation. This gives a junction voltage of $V=300\mu$V, and a difference between the two junction voltages, as a result of the gravitational red shift, of 2.35×10^{-21} V. Φ_m is essentially time independent except near the end of the run when the helium level is near the rf SQUID. This

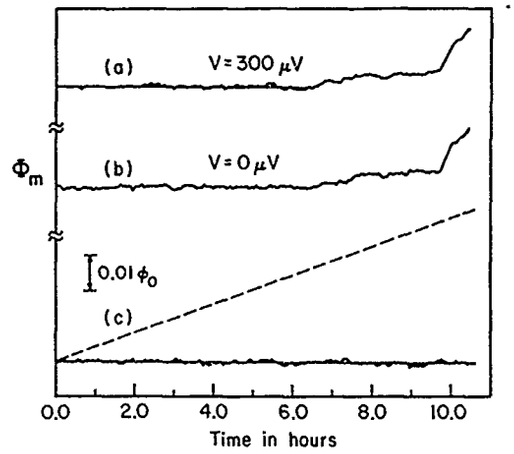

FIG. 2. Curve *a*, Φ_m vs time with the junctions phase locked to 16.8-GHz radiation biased at 300 μV on the ninth-order step. Curve *b*, Φ_m vs time with the junctions biased on the zeroth step. Curve *c*, $\Phi_m(V=300\ \mu\text{V})-\Phi_m(V=0\ \mu\text{V})$ vs time. The dashed line shows the expected signal if μ rather than $\tilde{\mu}$ remained constant along the superconducting wire. The solid lines in *a* and *c* are the respective best linear fits as described in the text.

dependence of Φ_m on time is highly reproducible from run to run. To check that the residual signal is due to the rf SQUID, the measurement was repeated with the junction bias current reduced so that the junctions were on their zeroth step (i.e., $V=0\ \mu$V). The resulting variation of Φ_m with time, shown in Fig. 2, curve *b*, is essentially identical to that in Fig. 2, curve *a*, indicating that there is no measurable change in the flux Φ through the sample loop during the run. The maximum flux change through the sample loop as a result of relativistic effects is just the difference between curves *a* and *b*, i.e., $\Phi_m(V=300\ \mu\text{V})-\Phi_m(V=0\ \mu\text{V})$ as shown in Fig. 2, curve *c*.

A linear-regression analysis of the data in Fig. 2, curve *c*, taking into account the presence of $1/f$ noise in the SQUID output, gives for the magnitude and error limits (2σ) of the loop voltage $(3\pm6)\times10^{-23}$ V. Nearly the same limits are obtained from the data in Fig. 2, curve *a*, if the final 4 h of data at low helium level are discarded. In this case we obtain $(1\pm8)\times10^{-23}$ V.

We thus conclude that the net emf in a superconducting loop containing two Josephson-effect batteries at different gravitational potentials is not the difference in the battery electrochemical potentials, $\Delta V=\lambda V$, but rather is indistinguishable from zero, consistent with the relativistic prediction that $\tilde{\mu}$ rather than μ is constant along the superconducting wires. In particular we have tested the hypothesis that the potential difference between the wires varies with height as $V(z)=V(0)\times(1-\lambda_q)$. Our results imply that $\lambda/\lambda_q=1\pm0.04$, as compared with the predicted equality of λ and λ_q

We would like to acknowledge useful conversations

with Jeeva Anandan as well as the assistance of Karen Springer in sample fabrication. This work was supported by the U. S. Office of Naval Research with additional support, for facilities used in this work, from the National Science Foundation under Grant No. DMR-86-40195, and the U. S. Air Force Office of Scientific Research.

---

[a]Present address. Central Research Laboratory, NEC Corporation, Kawasaki, Kanagawa 213, Japan.

[1]R. V. Pound and S. A. Rebka, Phys. Rev. Lett. **4**, 337 (1960).

[2]R. F. C. Vessot and M. W. Levine, Gen. Relativ. Gravitation **10**, 181 (1979), C. O. Alley, in *Quantum Optics, Experimental Gravity and Measurement Theory*, edited by P. Meystre and M. O. Scully (Plenum, New York, 1983), p. 363.

[3]J. Anandan, Phys. Lett. **105A**, 280 (1984).

[4]For a discussion of general relativistic effects in superconductors and references to earlier work, see J. Anandan, in *New Techniques and Ideas in Quantum Measurement Theory*, edited by D. Greenberger (N.Y. Academy of Science, New York, 1987), p. 224.

[5]R. M. Brady, Ph.D. thesis, University of Cambridge, 1982 (unpublished).

[6]J. Anandan, Class. Quantum Grav. **1**, L51 (1984).

[7]L. I. Schiff and M. V. Barnhill, Phys. Rev. **151**, 1067 (1966).

[8]A. J. Dessler *et al.*, Phys. Rev. **168**, 737 (1968).

[9]W. M. Fairbank, Physica (Amsterdam) **109B&110B**, 1404 (1982).

[10]A. K. Jain, J. E. Lukens, and J.-S. Tsai, Bull. Am. Phys. Soc. **31**, 495 (1986), gives preliminary results of these measurements.

[11]J. Clarke, Phys. Rev. Lett. **21**, 1566 (1968).

[12]J.-S. Tsai, A. K. Jain, and J. E. Lukens, Phys. Rev. Lett. **51**, 316 (1983).

[13]See, for example, K. K. Likharev, *Dynamics of Josephson Junctions and Circuits* (Gordon and Breach, New York, 1986), Chap. 10.

[14]The full general-relativistic treatment of fluxoid quantization may be found in Ref. 4. The treatment of gravitation as an additive effect to the nonrelativistic equations, presented here for simplicity, is equivalent in the limit of weak uniform fields applicable to this experiment.

VOLUME 63, NUMBER 16 PHYSICAL REVIEW LETTERS 16 OCTOBER 1989

Thermal Activation in a Two-Dimensional Potential

S. Han, J. Lapointe, and J. E. Lukens

Department of Physics, State University of New York at Stony Brook, Stony Brook, New York 11794

(Received 13 July 1989)

Measurements have been made of the transition rates between fluxoid states of a system with two Josephson junctions having two macroscopic degrees of freedom. The data, taken over a temperature range of 0.85 to 4.41 K, are in excellent agreement with the predictions for thermally activated transitions. No evidence is seen for recently reported apparent rate suppression below that predicted for thermal activation.

PACS numbers: 74.50.+r, 05.40.+j, 85.25.Cp

Josephson junctions have proven to be excellent systems in which to study the dynamics, both classical and quantum, of a macroscopic coordinate in a metastable potential. In general, careful experiments have yielded excellent agreement with theory for systems with one degree of freedom, i.e., a single, small junction. Recent results by Sharifi, Gavilano, and Van Harlingen[1,2] (SGV) on thermal activation from the zero-voltage state of a dc SQUID (a system with two degrees of freedom) have, however, shown marked disagreement with classical theory for two-dimensional (2D) potentials and have been interpreted as showing a dramatic suppression of the thermal activation rate from that predicted. In this Letter we report the results of thermal activation measurements on a similar two-dimensional system of Josephson junctions (a combined rf-dc SQUID) in which the potential can be independently determined to very high accuracy.

The system studied here, as shown in Fig. 1, consists of two Josephson junctions in parallel in a low inductance (l) superconducting loop (the dc SQUID) which is incorporated as part of a larger inductance (L) superconducting loop (the rf SQUID). The macroscopic dynamical variables which describe this system are the fluxes Φ (which can be monitored) and Φ_{dc} linking, respectively, the rf and dc SQUID's. The fluxes applied to these loops, Φ_x and Φ_{xdc}, can be independently controlled. The dynamics of this system can be visualized as motion in a 2D potential, which for symmetric dc SQUID having equal junctions is given by

$$U(\varphi,\varphi_{dc}) = \frac{\Phi_0^2}{4\pi^2 L}\left[\tfrac{1}{2}(\varphi-\varphi_x)^2+\tfrac{1}{2}\gamma(\varphi_{dc}-\varphi_{xdc})^2 - \beta\cos\tfrac{1}{2}\varphi_{dc}\cos\varphi\right], \quad (1)$$

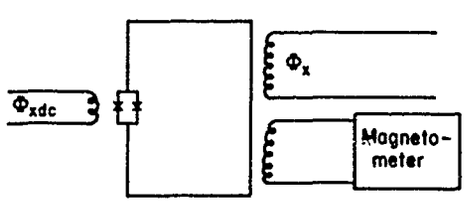

FIG. 1. Schematic of SQUID sample and coupling coils.

with a damping determined both by the junctions' resistance and the environment. Here, Φ_0 is the flux quantum, $\gamma \equiv L/l$ is the ratio of the loop inductances, and $\beta \equiv 2\pi L I_c/\Phi_0$, where I_c is the sum of the junctions' critical currents. $\varphi_{(\,)} = \Phi_{(\,)}[2\pi/\Phi_0]$. Figure 2 shows a plot of this potential for $\beta = 4.14$ and $\gamma = 19.5$ (the case for the junctions measured here) with $\Phi_x = 0.65\Phi_0$ and $\Phi_{xdc} = 0$. For these parameters the potential consists of two local minima connected by a saddle point. For the values of β and γ here, there are at most two local minima with $U(\Phi,\Phi_{dc})$ increasing roughly parabolically at large Φ and Φ_{dc}. For values of $\Phi_{xdc} > 0$ the barrier amplitude is reduced, finally going to zero for $\Phi_{xdc} = 0.405\Phi_0$ (for

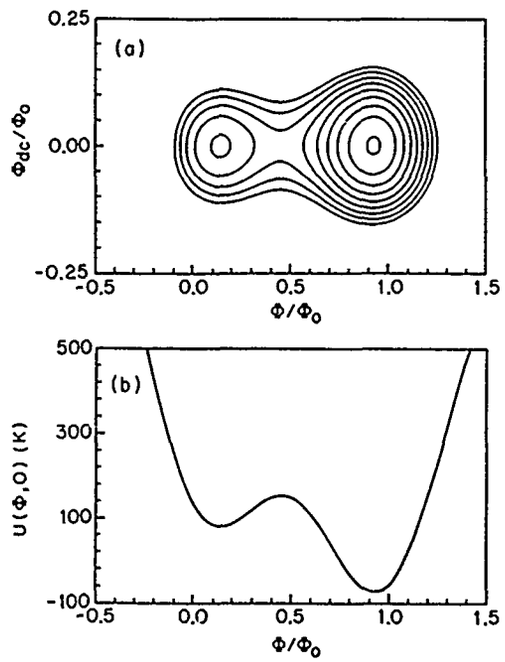

FIG. 2. The 2D potential $U(\Phi,\Phi_{dc})$ of our sample SQUID with symmetric dc SQUID having identical junctions. The mutual inductance between two loops is taken to be $l/2$. The potential for $\beta = 4.14$, $\gamma = 19.5$, $\Phi_x = 0.65\Phi_0$, and $\Phi_{xdc} = 0$ showing (a) equipotential contours at the above value of external fluxes and (b) $U(\Phi,0)$. U continues to increase monotonically (roughly parabolically) for greater values of Φ and Φ_{dc} than those shown.

© 1989 The American Physical Society

$\Phi_x = \frac{1}{2}\Phi_0$) so that no metastable states exist. Also for $\Phi_{xdc} > 0$ the path linking the wells through the saddle point is no longer a straight line. The details of this potential along with the techniques used for the measurement of its parameters will be presented in a forthcoming extended paper.

The longitudinal (transverse) small oscillation frequencies parallel (perpendicular) to the path from the well through the saddle point are ω_{lw} (ω_{tw}) in the well and ω_{ls} (ω_{ts}) at the saddle point. The predicted rate of thermally activated escape from such a two-dimensional well is given in the classical limit by Ben-Jacob *et al.*[3] to be

$$\Gamma_{2D} = \frac{\Omega}{2\pi} \exp[-\Delta U(\varphi,\varphi_{dc})/k_B T], \quad (2)$$

where ΔU is the energy difference between the metastable potential well and the saddle point and $\Omega = \Omega_0 a_t$. $\Omega = \omega_{lw}\omega_{tw}/\omega_{ts}$ and a_t is a damping-dependent suppression of the rate which can be much less than one in both high- and low-damping limits, i.e., for ω much greater or much less than RC. R and C are, respectively, the junction's resistance and capacitance. For moderate to heavy damping $a_t = (1+G^2/4)-G/2$, where $G = 1/RC\omega_{ls}$. In the extreme underdamped limit, $a_t \ll 1$ is also predicted since

$$a_t = \frac{2\pi\omega_{ts}}{\omega_{tw}} \frac{1}{RC\omega_{lw}} \left(\frac{\Delta U}{k_B T}\right)^2 .$$

Recent results for single-current biased junctions provide evidence for this extreme underdamped limit with a damping $\eta \propto \exp(-\Delta U/k_B T)$, where ΔU is the superconducting energy gap, as expected for quasiparticles.[4-6] However, the extension of these results to multidimensional potentials is still open to question.[7]

All measurements were made in highly shielded cryostats (either ^{4}He or dilution refrigerator). All signals were inductively coupled to the sample, which was enclosed in a NbTi can, through leads having low-temperature low-pass filters. For low-temperature measurements a resistive shunt, heat sunk to the dilution refrigerator mixing chamber, was placed across the magnetometer input to filter any high-frequency signals generated by the SQUID magnetometer. The junctions used were nominal 1×1 μm^2 $Nb/Al_2O_3/Nb$ tunnel junctions with very low subgap leakage. The *I-V* curve of an unshunted (without L) SQUID coprocessed with the sample SQUID is shown in the inset of Fig. 3(b). These data give a single-junction differential resistance of $R_n = 320$ Ω above the gap and a critical current of $I_c = 5.8$ μA. From the dc SQUID resonance of this unshunted SQUID with $\Phi_{xdc} > 0$, a capacitance of $C = 46 \pm 6$ fF was determined in agreement with the specific capacitance obtained by Lichtenberger *et al.* for similar junctions.[8] The inductance l of the dc SQUID was determined from the sample as discussed below.

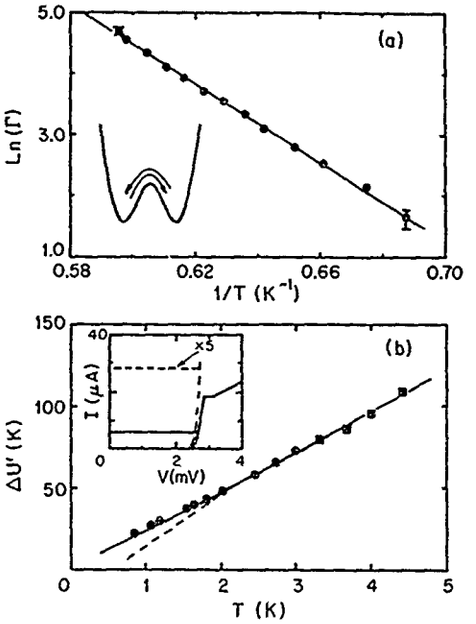

FIG. 3. Thermal activation rates between fluxoid states for the symmetric potential ($\Phi_x = \frac{1}{2}\Phi_0$) shown as the inset in (a). (a) Rate vs $1/T$ for fixed barrier height with best linear fit (line). (b) Barrier height vs T for fixed rate ($\Gamma = 1$ s^{-1}). For points indicated by squares, data have been corrected for temperature dependence of critical current. Best fit by Eq. (2) assuming damping due to R_n (solid line), or damping proportional to $\exp[-\Delta U/k_B T]$ from quasiparticles (dashed line). The inset of (b) shows the dc SQUID *I-V* curve for $T = 1.5$ K, $\Phi_{xdc} = 0$ indicating low subgap leakage.

For the special case where Φ_x is a half-integer flux quantum, the potential is symmetric about $\Phi = \Phi_x$ so that $\Delta U(\Phi_{xdc})$ is the same for each well [see inset, Fig. 3(a)], varying from a maximum of 143 K for $\Phi_{xdc} = 0$ to 0 for $\Phi_{xdc} > 0.405\Phi_0$, where the potential has only one minimum. Figure 3(a) shows the measured rate at which the sample hops between two equal energy fluxoid states versus temperature with constant ΔU (fixed Φ_{xdc}). If Ω is temperature independent in this range, one expects from Eq. (2) that a linear relationship exists between $\ln(\Gamma)$ and $1/T$ since

$$\ln(\Gamma) = -\Delta U/kT + \ln(\Omega/2\pi). \quad (3)$$

As Fig. 3 shows, the observed dependence is in fact linear, giving best-fit values of $\Delta U = 32.2 \pm 0.4$ K and $\ln(\Omega/2\pi) = 23.9 \pm 0.3$. These agree well with the values of $\Delta U = 33.5 \pm 3$ K and $\ln(\Omega/2\pi) = 24.4 \pm 0.2$ calculated from measured sample parameters, as discussed below. Here $a_t = 1$ has been used; taking the damping to be $1/R_n$ would give $a_t \approx 0.9$—an insignificant correction.

The greatest uncertainty in the calculated value of ΔU comes from the knowledge of L, which has been calculated from the loop geometry, giving $L = 230$ pH ± 10%. Measurements on single-junction SQUID's[9,10] have shown such calculations to be reliable for the geometry

used here. Both γ and the difference in the junctions' critical currents, $\delta \equiv (I_2 - I_1)/I_c$, can be determined from the equilibrium dependence of Φ on Φ_x measured when Φ_{xdc} is a half-integer flux quantum so that the system has no metastable states. These data give $\gamma = 19.5$ and $\delta < 5\%$ justifying the treatment of the junction parameters as equal. β is determined by measuring the value of Φ_x at which the system escapes from its metastable state for $\Phi_{xdc} = 0$. Since this escape will occur slightly before the barrier is reduced to zero, a small, model-dependent correction to β based on Eq. (2) is required. This correction, at most, increases the calculated ΔU above by 5% over that which would be obtained by assuming the escape occurred for $\Delta U = 0$.

The transition rate as shown in Fig. 3(a) is only measurable over a narrow range of temperature for fixed ΔU. To measure the temperature dependence of this rate over a broad range of temperature, ΔU was adjusted at each temperature to give approximately the same rate, $10 < \Gamma < 50$. These data are plotted as $\Delta U'$ vs T in Fig. 3(b). Here $\Delta U' \equiv \Delta U + k_B T \ln[\Gamma/1\ s^{-1}]$ is the measured barrier normalized for the small variations in $\ln(\Gamma)$ among the points. Again $\Phi_x = \frac{1}{2}\Phi_0$ and $\Delta U(\Phi_{xdc})$ was adjusted by varying Φ_{xdc} and calculated from the parameters as above.

The theoretical curve for thermal activation has been plotted using Eq. (3) taking the damping to be $1/R_n$ which gives $a_t \approx 0.9$. The uncertainty in the independently measured values of $\Delta U \pm 10\%$ implies an acceptable fit to the data in Fig. 3(b) for any temperature-independent damping less than $0.05\ \Omega^{-1}$ if the moderate damping expression for a_t is used. The dashed line in Fig. 3(b) is calculated assuming the damping $\eta \propto \exp(-\Delta U/k_B T)$ as expected for quasiparticles and using the extreme underdamped expression for a_t. This is not consistent with our data, however, we emphasize that this result may imply only that extrinsic damping (e.g., losses from the SQUID loop) dominates.

We conclude that the data presented in Fig. 3 are entirely consistent with thermal activation [Eq. (2)] and, in particular, do not admit an effective barrier height

TABLE I. Characteristic energies (in units of kelvin) of the symmetric double-well potential ($\Phi_x = \frac{1}{2}\Phi_0$) which describes the system for data in Fig. 3. At each temperature Φ_{xdc} has been adjusted to give the values of ΔU shown.

	$T = 0.85$ K	$T = 4.41$ K
ΔU	18	92
$\hbar\omega_{lw}$	1.85	3.15
$\hbar\omega_{tw}$	14.6	14.8
$\hbar\omega_{ls}$	1.36	2.61
$\hbar\omega_{ts}$	14.4	14.2
$\Delta U/\hbar\omega_{lw}$	9.7	29
$\Delta U/\hbar\omega_{tw(s)}$	-1.2	-6

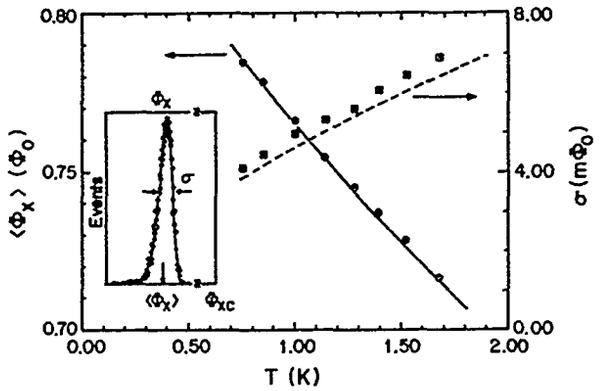

FIG. 4. Mean $\langle\Phi_x\rangle$ (circles) and width σ (squares) of the thermal activation probability distribution (see text) vs T at $\Phi_{xdc} = 0.122\Phi_0$. The solid and dashed lines are, respectively, the predicted mean and width from Eq. (2) using parameters given in text. Inset. A typical distribution used to calculate $\langle\Phi_x\rangle$ and σ at one temperature.

$\Delta U^* = 2.5\Delta U$ as needed by SGV to explain their data in the thermal activation regime. The energies associated with the symmetric potential over the temperature range of the measurements are summarized in Table I. For comparison, we note that both for these data and for those of SGV, $\hbar\omega_l \approx k_B T$, whereas $\hbar\omega_t \gg k_B T$ with $\omega_t/\omega_l \approx 8$. Even for our lowest-temperature data there are at least ten energy levels in the wells, satisfying the validity criteria for the classical [Eq. (2)] and semiclassical[11] rate calculations. The expected crossover temperature T_x for tunneling-dominated transitions is $T_x = 0.35$ K in the zero-damping limit. Thus quantum correction[11] to Eq. (2) should be negligible for our data. Naor, Tesche, and Ketchen[12] have also reported excellent agreement with thermal activation theory for their measurements for transitions for $T > 1.7$ K in a highly damped, current-biased dc SQUID with $\omega_t/\omega_l \approx 1$.

A more direct comparison with the results of SGV is provided by the data in Fig. 4. Here, for $\Phi_{xdc} = 0.122\Phi_0$, Φ_x is increased at a constant rate reducing the barrier height until the SQUID undergoes a change of fluxoid state by escaping from a metastable well. Measurements of this type on a single-junction SQUID have been described in detail elsewhere.[9,10] These measurements are repeated approximately 10^4 times at a fixed temperature giving a histogram of transition probability versus Φ_x (see Fig. 4, inset). The first and second moments of this distribution, $\langle\Phi_x\rangle$ and σ, respectively, are predicted to vary with temperature[13] as shown by the solid and dashed lines in Fig. 4 assuming a potential and transition rate given by Eqs. (1) and (2) and using the sample parameters above.

In calculating $\langle\Phi_x\rangle$ vs T the critical applied flux Φ_{xc} at which $\Delta U = 0$ is used as a temperature-independent fitting parameter, $\Phi_{xc} = 0.882\Phi_0$, which is consistent with β measured for $\Phi_{xdc} = 0$. As can be seen, the agree-

ment with thermal activation predictions is excellent. This contrasts with similar measurements by SGV in which they found for their system that $d\langle\Phi_x\rangle/dT$ was about a factor of 3 less than predicted. The width σ also varies with temperature as expected, although it is about 5% greater than predicted. This is consistent with the excess width expected from the Nyquit flux noise on the sample due to the shunt resistor across the magnetometer. The temperature of this shunt varied from 50 to 180 mK as the sample temperature was increased.

Measurements have been made of thermally activated transitions between fluxoid states of a SQUID system having two macroscopic degrees of freedom, in which the energy potentials could be accurately determined and where existing classical and semiclassical theory should be valid. Excellent agreement has been found with the prediction of thermal activation theory. In particular, no hint was seen of the very large apparent rate suppression recently reported in a similar system by SGV. In view of the similarities of the potentials for these two measurements (in particular, the ratios of the longitudinal and transverse level spacing to k_BT), our results should serve to focus on the key features of the system used by SGV responsible for their anomalous results. For example, our results indicate that such anomalies cannot be a general feature of two-dimensional potentials even in the limit where $\hbar\omega_t \gg k_BT$ so that level quantization of the transverse mode is important.

We would like to acknowledge the contributions of C. N. Archie, Aloke Jain, and B. Sen in the initial stages of this work as well as numerous helpful conversations with S. Chakravarty and S. Kivelson. This work was supported by the U. S. Office of Naval Research.

[1]F. Sharifi, J. L. Gavilano, and D. J. Van Harlingen, Phys. Rev. Lett. **61**, 742 (1988).

[2]F. Sharifi, J. L. Gavilano, and D. J. Van Harlingen, IEEE Trans. Mag. **25**, 1174 (1989).

[3]E. Ben-Jacob, D. J. Bergman, Y. Imry, B. J. Matkowsky, and Z. Schuss, J. Appl. Phys. **54**, 6533 (1983); C. D. Tesche, J. Low Temp. Phys. **44**, 119 (1981).

[4]P. Silvestrini, S. Pagano, Roberto Cristiano, O. Liengme, and K. E. Gray, Phys. Rev. Lett. **60**, 844 (1988).

[5]P Silvestrini, O. Liengme, and K. E. Gray, Phys. Rev. B **37**, 1525 (1988).

[6]J. R. Kirtley, C. D. Tesche, W. J. Gallagher, A. W. Kleinsasser, R. L. Sandstrom, S. I. Raider, and M. P. A. Fisher, Phys. Rev. Lett. **61**, 2372 (1988).

[7]R. Landauer (private communication); S. Kivelson (private communication).

[8]A. W. Lichtenberger, C. P. McClay, R. J. Mattauch, M. J. Feldman, S. K. Pan, and A. R. Kerr, IEEE Trans. Mag. **25**, 1247 (1989).

[9]D. B. Schwartz, B. Sen, C. N. Archie, and J. E. Lukens, Phys. Rev. Lett. **55**, 1547 (1985).

[10]D B Schwartz, Ph.D. thesis, State University of New York at Stony Brook, 1986 (unpublished).

[11]H. Grabert, P. Olschowski, and Ulrich Weiss, Phys. Rev. B **36**, 1931 (1987).

[12]M. Naor, C. D. Tesche, and M. B. Ketchen, Appl. Phys. Lett. **41**, 202 (1982).

[13]J. Kurkijärvi, Phys. Rev. B **6**, 832 (1972).

Final report on ONR contract #N00014-84-C-0261

List of Publications

"Length Dependent Properties of SNS Microbridges," J.E. Sauvageau, R.H. Ono, A.K. Jain, K. Li, and J.E. Lukens, IEEE Trans. on Mag., **MAG-21**, 854 (1985).

"Suspended Metal Mask Techniques in Josephson Junction Fabrication," R.H. Ono, J.E. Sauvageau, A.K. Jain, D.B. Schwartz, K.T. Springer, and J.E. Lukens, J. Vac. Sci. Tech. B, 3(1), (1985).

"The Decay of Metastable States in Systems with Highly Damped Josephson Junctions," D.B. Schwartz, B. Sen, C.N. Archie, A.K. Jain, and J.E. Lukens, *Proceedings of the Third IC SQUID Conference*, Berlin (June 1985).

"Quantitative Study of the Effect of the Environment on Macroscopic Quantum Tunneling," D.B. Schwartz, B. Sen, C.N. Archie, and J.E. Lukens, Phys. Rev. Lett. 55, 1547-1550 (1985).

"Phase-locking in Distributed Arrays of Josephson Oscillators," J.E. Sauvageau, A.K. Jain, and J.E. Lukens, IEEE Trans. on Mag., **MAG-23**, No. 2, 1048-1050 (1987).

"Variation of the Electrochemical Potential Difference in a Gravitational Field," A.K. Jain, J.E. Lukens, and J.-S. Tsai, IEEE Trans. on Mag., **MAG-23**, No. 2, 450-453 (1987).

"Test for Relativistic Gravitational Effects on Charged Particles," A.K. Jain, J.E. Lukens, and J.-S. Tsai, Phys. Rev. Lett. 58, 1165-1168 (1987).

"Submillimeter wave generation using Josephson junction arrays," K. Wan, A.K. Jain, and J.E. Lukens, Appl. Phys. Lett. 54, 1805-1807 (1989).

"Thermal Activation in a Two-Dimensional Potential," S. Han, J. Lapointe, and J.E. Lukens, Phys. Rev. Lett. 63, 1712-1715 (1989).

"Josephson Arrays as High Frequency Sources," Chapter 4 in *Modern Superconducting Devices*, S. Ruggiero and D. Rudman, Eds., Academic Press, Boston, 1990.

"Observation of Final State Effects on Macroscopic Quantum Transitions," J. Lapointe, S. Han, J. Lukens, to be published in *Proceedings of LT–19.*

"Observation of Incoherent Relaxation by Tunneling in a Macroscopic Two-State System," S. Han. J. Lapointe, and J.E. Lukens, submitted to Physical Review Letters.

Final report on ONR contract #N00014-84-C-0261

List of students with ONR support receiving Ph.D.s

Peter Kopietz

Joseph Sauvageau